Project Number: <ME-RLN-0801>

Inserter Mechanism Redesign

A Major Qualifying Project Report

Submitted to the Faculty

of the

WORCESTER POLYTECHNIC INSTITUTE

in partial fulfillment of the requirements for the

Degree of Bachelor of Science

in Mechanical Engineering

by

Kenneth Barnett Nicole Nelson Corey Randall Mark Rizzo

_____ _____ _____ _____

Date: December 18, 2008

Approved:

_____

Prof. Robert L. Norton, Advisor

Keywords:
1. Assembly machine
2. Cam design
3. Machine design
4. Slider mechanism

Acknowledgements

The MQP team would like to thank the following individuals from WPI and the sponsoring company for their commitment and assistance throughout the course of this project:

- Professor Robert Norton
- Professor Eben Cobb
- Professor Holly Ault
- Randolph Robinson
- Charles Gillis
- Corey Maynard
- Stephen Kilkelly
- Ernie Chandler
- Frank Finneran
- Kenneth Bellibeau

Abstract

This project redesigned components that were causing occasional binding of a cam-driven product inserter station on an assembly machine at the sponsoring company. The device consisted of a vacuum gripper and set of mechanical strippers guided by telescoping slides whose strokes were limited by a series of hard stops. We created parametric and dynamic models of the mechanism using CAD and FEA software, gathered experimental data using accelerometers, and examined the assembly through high-speed video and physical inspection. We discovered that the binding occurred within the inner slider assembly, where one of the hard stops applied large forces and moments and caused excessive wear to the sliding surfaces. We redesigned the assembly to increase the slide's bearing ratio and decrease the effect of the applied moment. Also, we implemented a new cam and observed a 17% decrease in acceleration during the hard stop and a 4.6% decrease in RMS acceleration over one cycle. We are confident that our redesign, if fully applied, would effectively eliminate the binding.

Executive Summary

This project examined and redesigned an occasionally malfunctioning machine station at the sponsor's manufacturing facility. The mechanism was used to pick up individual products from an indexing nest conveyor and insert them into containers for end use. The device consisted of a vacuum gripper and set of mechanical strippers guided by telescoping slides whose strokes are limited by a series of hard stops. The inner slide assembly on device was sporadically binding. When this happened, the assembly had to be dismantled, cleaned, and re-lubricated, resulting in significant productivity loss. We used models and various analyses to develop a redesign that would alleviate the binding issue.

Pro/Engineer computer models were created and used to simulate the motion as well as to obtain mass properties of the components in the mechanism. The models were then imported into SolidWorks for finite element analysis in order to determine the stiffnesses of various elements. This mass property data and part stiffnesses were then used to create a lumped model to analyze the vibration responses of the cam follower system. Accelerometer test data were then taken to verify the accuracy of the dynamic simulation.

The test data revealed spikes in acceleration during the two hard stops. The stop for the inner slide was cantilevered from the slide body, which caused a large moment to be applied to the slide during the hard stop impact. We inspected the assembly and observed evidence of premature wear on areas of the sliding surfaces where the moment was being applied from the hard stop. Furthermore, we found excessive wear on the nest-conveyor guide rail that served as the stop's anvil. We also noticed that the slide was designed with a very poor bearing ratio throughout its stroke. We determined that the combination of heavy loading and inadequate bearing ratio was most likely the root cause of the binding issue.

Our redesign focused on these factors. The inner slide was made longer and narrower to improve its bearing ratio. The length that was added to the slide was compensated for by shortening the assembly's connecting rod and moving the mounting bracket up. This was done to maintain the originally designed positioning of the end effector during the machine's cycle.

The slider assembly's hard stop was also redesigned to accommodate the longer slide. We incorporated into the station's weldment a reinforced ledge with a removable wear pad located in the precise position where the stop needed to be engaged. Although not directly related to the binding issue, the new weldment design prevents further damage to the nest guide rail and makes it easier to adjust the stop position during final assembly.

The final part of our redesign reduced the impact force applied to the assembly by decreasing the cam's velocity during the inner slide's hard stop. The cam was manufactured and tested on the machine. The data showed a 17% decrease in acceleration during the inner slide hard stops and a 4.6% decrease in RMS acceleration over one cycle. These results showed that the cam redesign had a positive effect on the impact and overall forces on the system.

The lead time needed to manufacture the redesigned slider assembly prohibited us from producing it and testing it on the machine during our seven week residency at the sponsor's company. However, we are confident that our redesign, if fully implemented, will effectively eliminate the binding. Consequently, the machine will operate more reliably and require less maintenance.

Table of Contents

List of Figures

List of Tables

1 Background

The sponsoring company's new product is manufactured on a fully automated production line in their manufacturing plant. One mechanism on the machine transfers the completed product from the inspection system into its packaging on a parallel conveyor system. This mechanism uses cam-driven tools, such as a vacuum gripper to hold the product and a mechanical stripper to release it. The mechanism regularly experiences binding which results in noise during operation and incorrect packaging of the product. When this happens the mechanism needs to be disassembled, cleaned, and lubricated, causing lost production time.

This mechanism consists of two independent cam linkage systems that work together to move the product. The nest opener is a cam driven system used to release the product from the inspection conveyor system and can be modeled as a four bar slider linkage. The inserter system consists of a cam follower system with an inner slide (vacuum head slide) on a main slide. The cams are driven from the same shaft, so their motions are coupled. The slides are controlled by the inserter cam, springs, and hard stops. It is the inner slider that is experiencing binding.

The inserter system is timed so the vacuum gripper makes contact with the product before the nest opener system activates the release button. To release the product from the conveyor, a tappet compresses a spring-activated release button that opens the jaws holding the product. Once connected, the gripper moves the product lightly into the product container. The movement of the vacuum gripper (shown in Figure 1.1) is halted by the first hard stop that hits the rail. Once the gripper system is stopped, the mechanical strippers insert the product firmly into the product container. To prevent damaging the product, the mechanical strippers are impeded by a second hard stop. The vacuum grippers then move upward and into a dwell to wait for the next product. Once the inserter system is clear of the nests, the tappet is released in order to let the nest close and the next nest come into place.

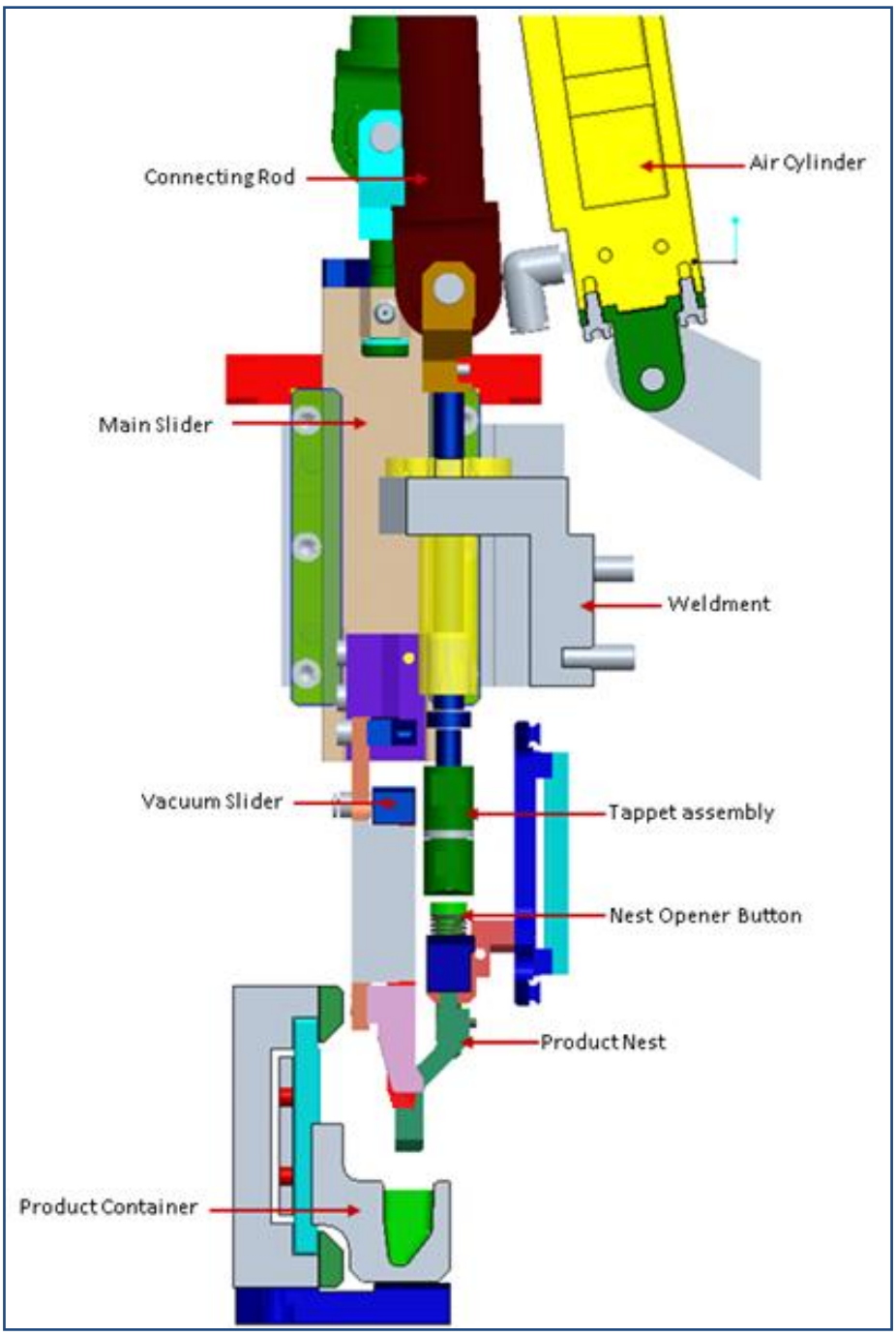

Figure 1.1: Product Inserter assembly

Air cylinders are used to provide the force to close the follower on the cam. In the event of a product failing inspection or being damaged, both sub-systems will be "locked out". A lockout is achieved by a pressure reversal in the follower's air cylinders, causing the follower to come off the cam and be disabled for one cycle.

1.1 Nest Opener System

The nest opener system, shown in Figure 1.2, consists of several sections: the tappet assembly, follower assembly, air cylinder, and a connecting rod (conrod). The tappet assembly, which is the section of importance, is composed of the tappet and pushrod. The follower assembly consists of the cam follower lever (bellcrank lever), a bearing, and various connectors. The follower assembly is attached to the bearing housing and relates the motion of the cam to the conrod. The conrod then transfers the motion to the tappet assembly.

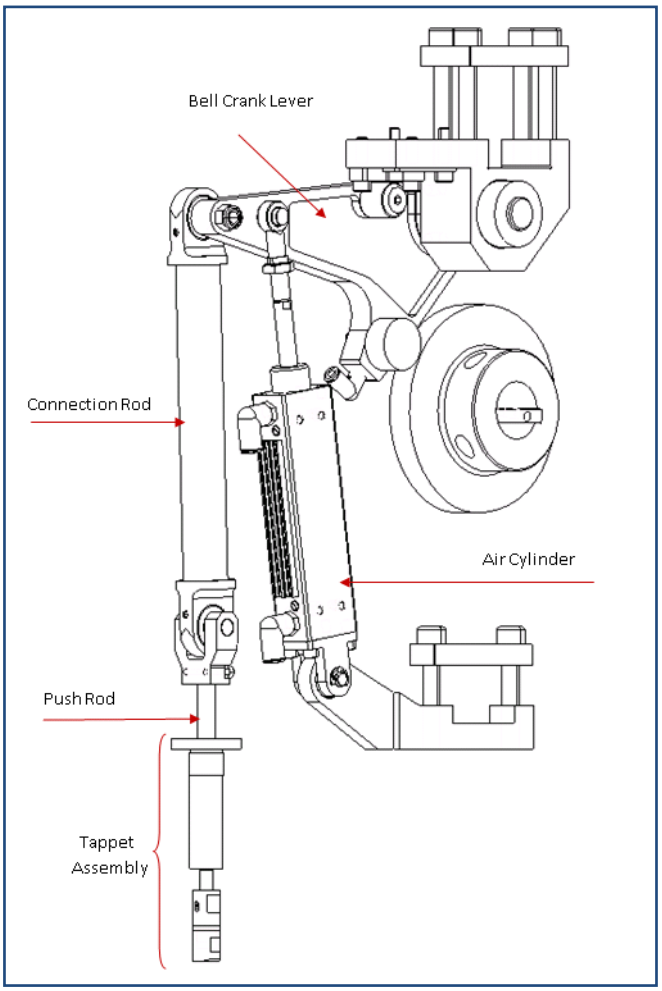

Figure 1.2: Nest Opener System, including corresponding cam

The tappet assembly moves in a purely vertical direction and is guided by a segment of the weldment. The function of the nest opener system is to activate the release button for the products. The button is on top of the nests of the unload/inspection conveyor and controls the opening of the jaws that hold the products in the nests. Tooling on the product inserter system will begin to hold the product before it is released. The timing for this is controlled by the two cams which are coupled on a single drive shaft.

1.2 Product Inserter System

The inserter system, shown in Figure 1.3, consists of the vacuum head assembly, main slide assembly, and conrod. The head assembly is composed of the slider housing, the vacuum head slider, and the section with the mechanical strippers, as depicted in Figure 1.4. The slider housing is connected to a weldment.

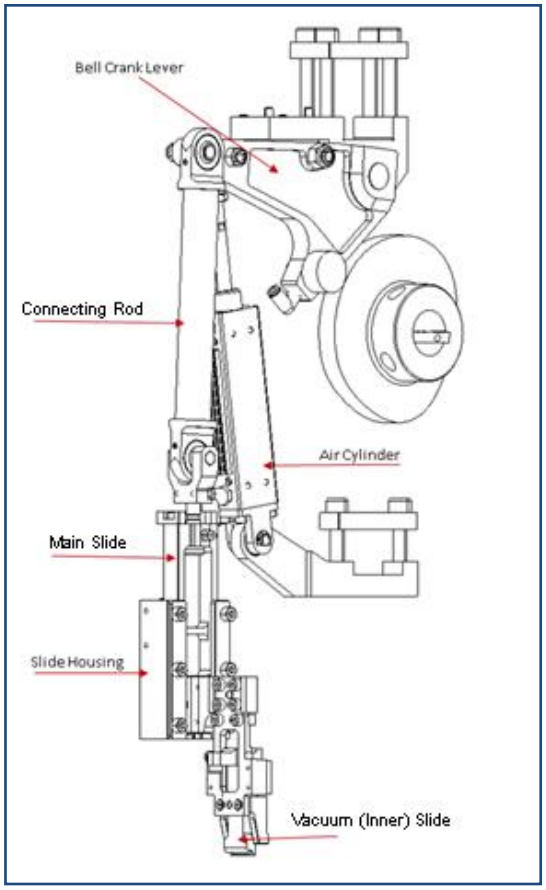

Figure 1.3: Inserter System, including corresponding cam

In the inserter system, motions of both the vacuum gripper and the mechanical stripper are caused by the same cam. The movement of the inserter system can be separated into three parts: contact with the product, contact with the first hard stop, and contact with the second hard stop. These critical locations defined points where the cam profile needed to be brought to a dwell or to a slower velocity.

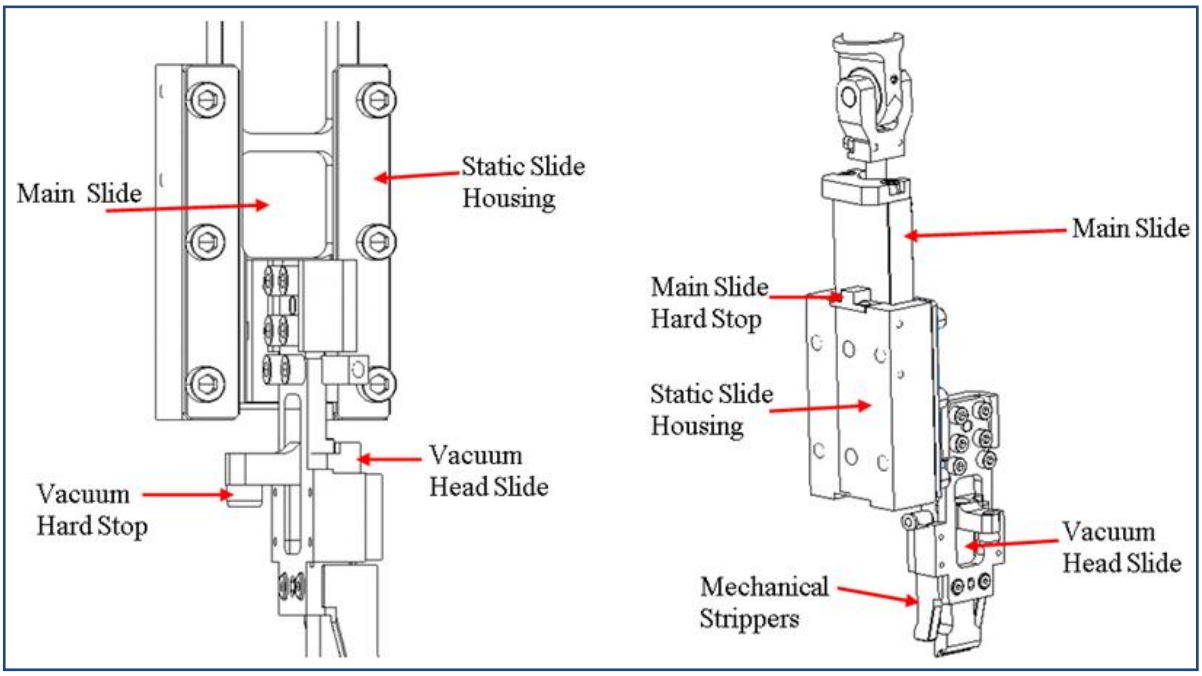

Figure 1.4: Inserter assembly close-up

At the initial dwell, the cam places the vacuum slider assembly above the nest. This allows time for the product container and nests to move on an indexed conveyor. Once the conveyor is in a dwell, the vacuum slider assembly and main slider move down to the product and rest for a very short period of time. The dwell allows the slider tooling to gain vacuum on the product and hold it. The nests then open, the slider resumes moving and the assembly continues down until the first hard stop. This hard stop occurs between the vacuum slider hard stop and a rail that is found on an adjacent station (see Figure 1.5). At this time, the vacuum head slide and the product stop. The main slide assembly continues downward until it hits its hard stop. Since the main slide assembly is continuing downward, the product is stripped away from the vacuum slide, breaking the vacuum on the product. The main slide hard stop then causes the assembly to stop moving downward. The need for this hard stop is

to keep a minimum critical dimension between the mechanical stripper and the product, avoiding collisions and damage to the product.

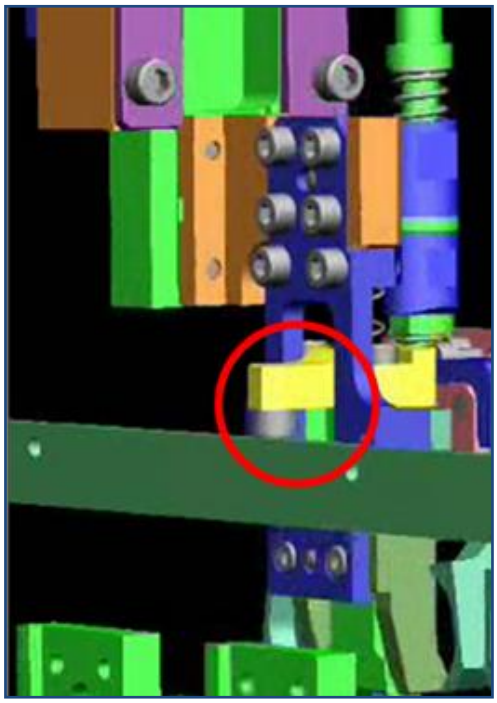

Figure 1.5: Vacuum Slider on its hard stop

2 Goal Statement

The product inserter mechanism regularly experiences binding which results in noise during operation and products that fail to go into the containers fully. The cams and linkages in this station need to be modeled and analyzed to determine what aspects of their design may be contributing to the problem. Then appropriate parts will be redesigned to improve their function.

3 Modeling

We created several models of the mechanism in order to properly understand its function and to predict the affects of making modifications to its design. A CAD model consisting of the entire product inserter station was modeled in Pro/Engineer. This parametric model allowed us to observe the relationships between different linkages and to view the overall motion of the mechanism. Moreover, it provided mass properties of all modeled components based on their geometry and material.

We also developed kinematic and dynamic models using Program DYNACAM. The kinematic model gave the motions of the cam follower without accounting for the vibrations caused by the rest of the linkage. This idealization served as a theoretical model of the system. We then developed a lumped parameter dynamic model to simulate how the masses and stiffnesses of the links affect the cam follower system. This provided dynamic force information necessary for evaluating vibrations and determining cam loading and follower separation characteristics.

3.1 CAD Model

We created a CAD model, shown in Figure 3.1, to observe the motions of the linkages and perform finite element analysis (FEA) on necessary components. The parts were modeled in Pro/Engineer from detailed drawings provided by the sponsor. The cams were created by generating their profiles in DYNACAM, exporting their surface profile points as text files, and importing these points into Pro/Engineer. Materials were assigned to every component in order to provide the mass properties needed for the dynamic analysis. The parts were then assembled using appropriate connection constraints and servo motors were applied to the cams and conveyors based on the running speed of the machine. The result was a 3D model that accurately simulates the physical motion of the mechanism.

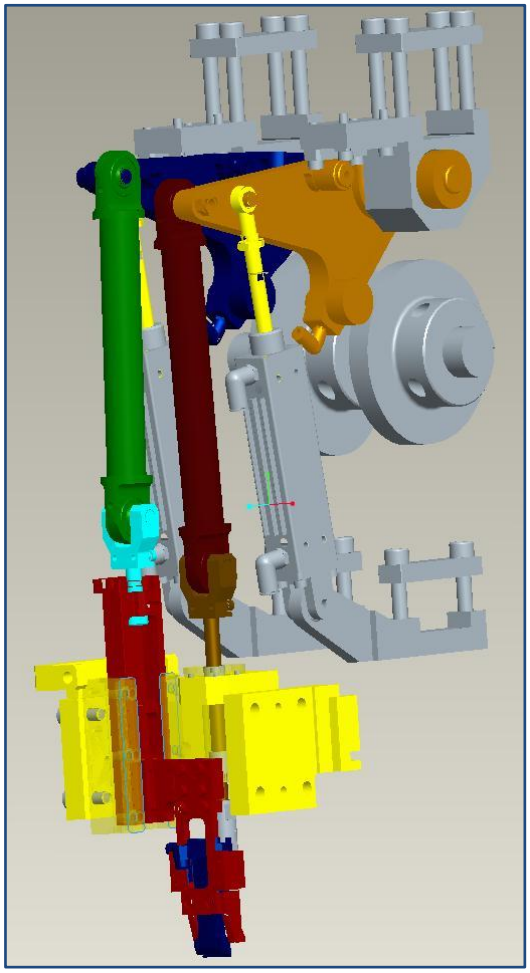

Figure 3.1: Inserter Mechanism CAD model (existing design)

3.2 Theoretical Motion Model

We were given DYNACAM files for the inputs needed to generate the profile of each existing cam. The information included segment lengths as well as the functions and boundary constraints that define each rise and fall action. Segment data, follower motion, and cam profile for the product inserter and nest opener cams are shown in Figure 3.2 through Figure 3.7.

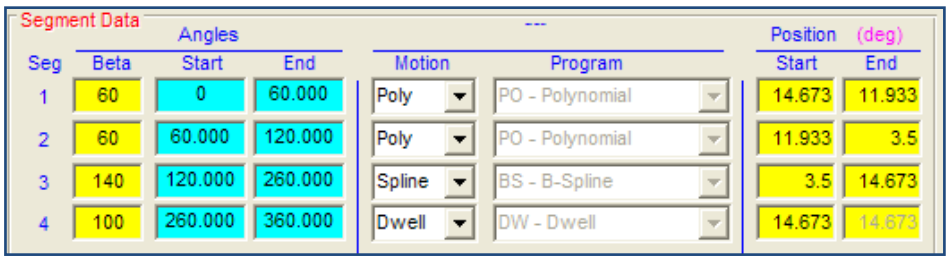

Figure 3.2: Inserter cam input data (existing design)

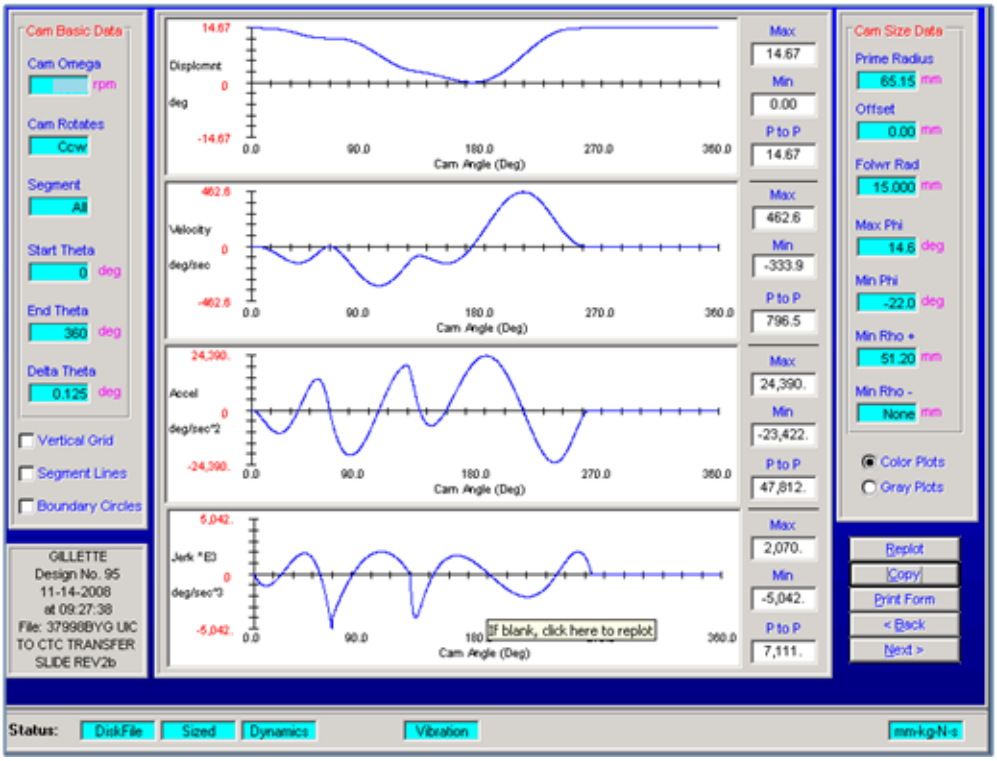

Figure 3.3: Inserter cam follower motion (existing design)

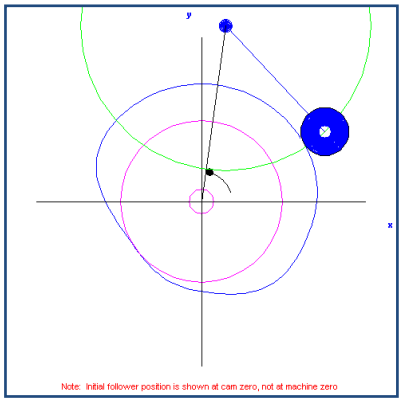

Figure 3.4: Inserter cam profile (existing design)

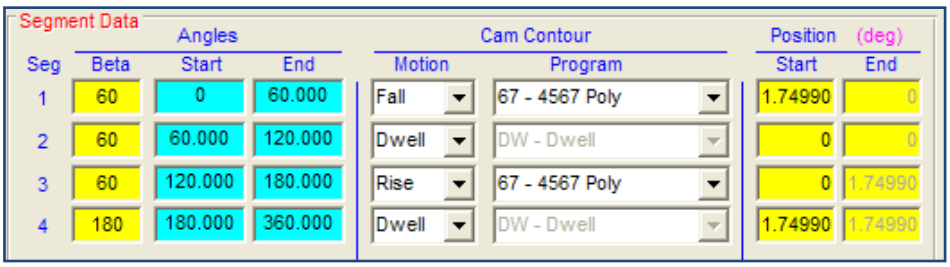

Figure 3.5: Nest Opener cam input data (existing design)

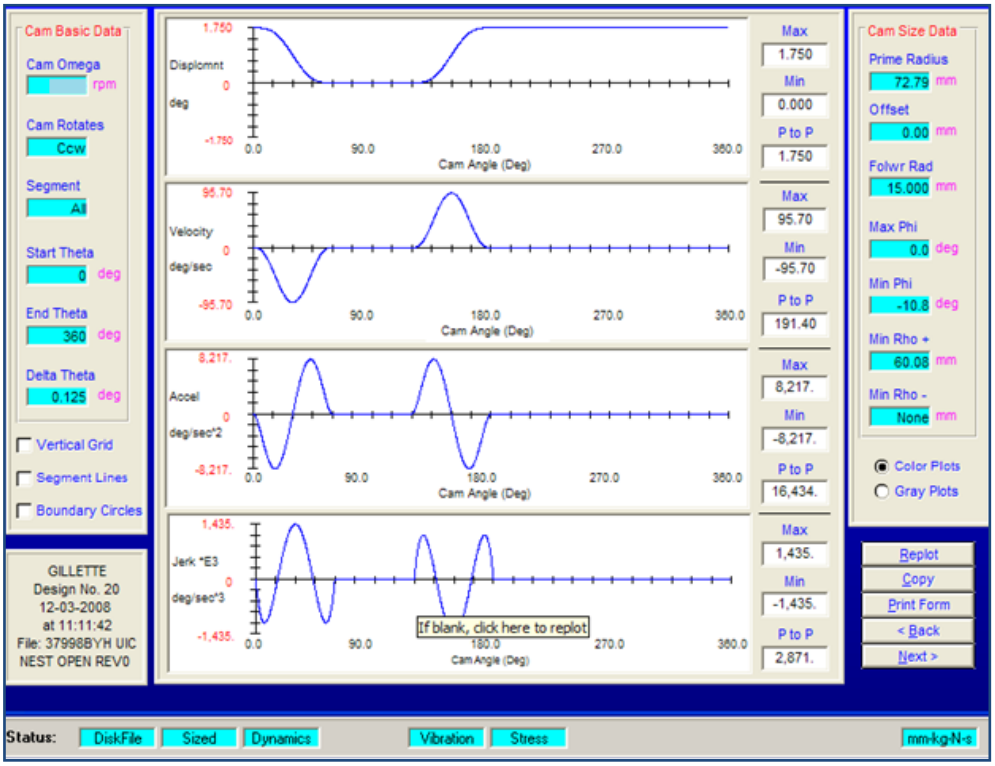

Figure 3.6: Nest Opener cam follower motion (existing design)

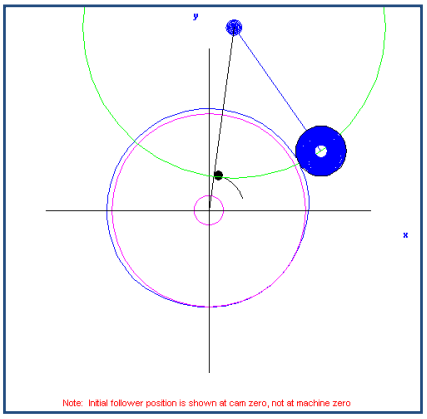

Figure 3.7: Nest Opener cam profile (existing design)

3.3 Dynamic Motion Simulation

To model the dynamic motion of the mechanism, we simplified the multitude of connected masses, springs, and sources of damping by creating a one-mass single-DOF model for each subsystem, as shown in Figure 3.8. Parameter k_1 is the spring constant of the air cylinder and k_2 is the combined stiffness of the follower train. The mass of each link is lumped into a single effective mass located at the roller follower. This is an appropriate model because the joint-closure spring (air cylinder) acts to close to the cam, and a significant amount of follower mass is downstream of the joint-closure spring.

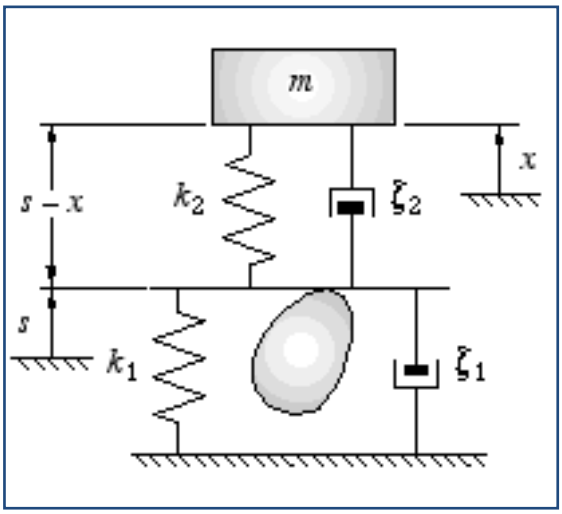

Figure 3.8: One-mass SDOF model

The spring constants for the links with complicated geometry were determined using SolidWorks FEA software, while the axial stiffness for the geometrically simple conrod was found by hand calculation. These data are shown in Appendix A. Every component that was analyzed with FEA was done so in a similar way. First, each part/assembly was imported into SolidWorks and given a material assignment. Then, appropriate restraints (such as fixed, hinge, and roller/sliding) and a force were applied to the model based on the physical characteristics of the system. Although some components underwent complex loading in reality, to obtain stiffness we generally applied a single force of realistic magnitude at the connection point or impact area of interest. Any reasonable value could be used for the applied force since the spring constant of a rigid body is linear for relatively small

deflections, according to Hooke's Law. The magnitude of the applied force was then divided by the resultant displacement generated by the FEA software to approximate that component's spring constant. An example of our general FEA setup is depicted in Figure 3.9. The image shows the restraint/loading arrangement and a representation of the displacement gradient for the vacuum head slider assembly, in which the most extreme displacement is shown in red. For the bellcrank (Figure 3.10), the loading point was offset laterally from the center of the pin hole to represent the twist caused by the conrod's offset.

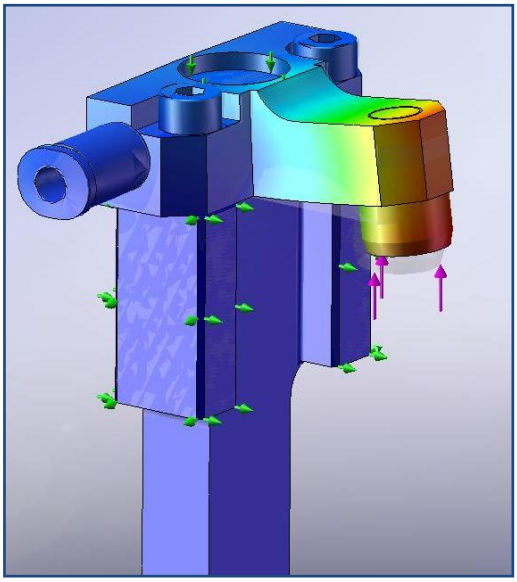

Figure 3.9: Vacuum Head Slider FEA setup and displacement gradient

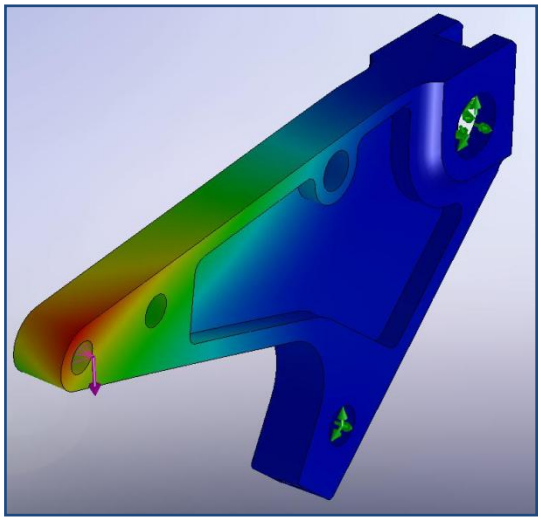

Figure 3.10: Bellcrank FEA setup and displacement gradient

As expected, the components with long moment arms, such as the bellcrank, were the least stiff; while the short, axially loaded components, such as the tappet, were the stiffest. This part of the analysis directed us to the weakest components in the machine and provided us a baseline with which to compare new designs. The spring constants for all the components were combined in series with lever ratios where applicable to find the overall spring constant for both linkage trains, as shown in Appendix B.

To determine the effective mass, we first found the masses of all the links using the Pro/Engineer models. Figure 3.11 shows how we separated the inserter system into a set of combined masses, each with its own spring constant. Since the masses of the conrod, yoke, and slider assemblies translate in essentially a straight line, their individual masses were simply added together and incorporated as a single mass located at the connection point on the bellcrank. To move its effects to the roller follower, this mass was multiplied by the square of the lever ratio of ***a*** to ***c***. The bellcrank's effective mass was found by multiplying its actual mass by the lever ratio of ***b*** (CG-pivot) to ***c***. The two effective masses were summed to produce the total equivalent mass for the SDOF model. These calculations are shown in Appendix B.

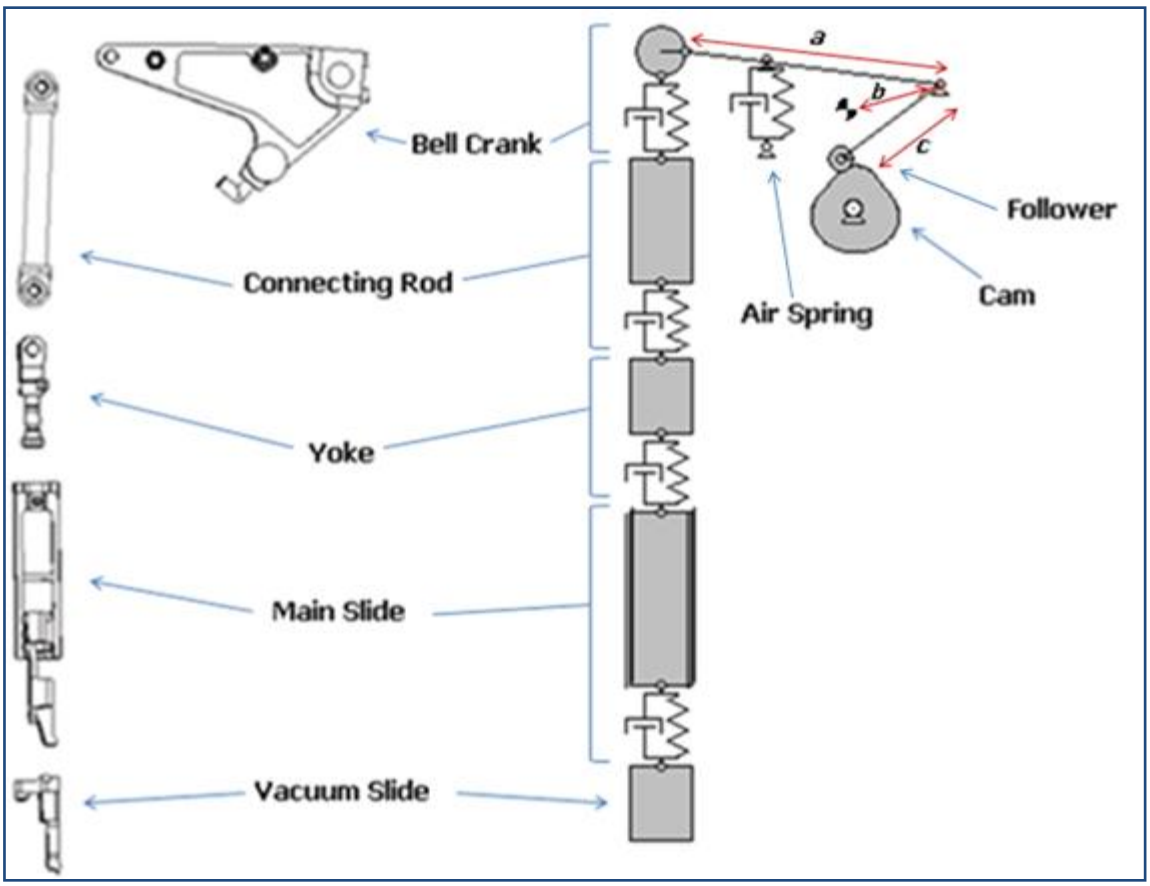

Figure 3.11: Lumped model of Inserter assembly

Table 3.1 shows the effective mass and stiffness of the mechanism components. These values were put into DYNACAM as parameters in our vibration simulation. We used a rough approximation for the friction in each subsystem by setting the damping to be 5% of critical damping for both the follower train and air cylinder. Figure 3.12 shows the displacement, velocity, and acceleration of the inserter cam-follower taking vibrations into account. Since the system had such a high effective stiffness, the simulation showed practically no vibratory oscillation. Thus, the kinematic and dynamic models appear very similar.

Table 3.1: Masses and stiffnesses of system components

	Name	Mass (kg)	Stiffness (N/m)
Inserter System	Vacuum Slider	0.156	4.32E+07
	Main Slider	0.892	1.25E+07
	Yoke	0.145	6.30E+08
	Connecting Rod	0.403	5.92E+08
	Bell Crank	1.766	9.29E+06
	Effective Mass and Stiffness at Follower	**6.832**	**1.87E+07**
Nest Opener System	Tappet	0.043	8.68E+08
	Pushrod/Yoke	0.201	1.24E+08
	Connecting Rod	0.470	5.45E+08
	Bell Crank	1.766	9.29E+06
	Effective Mass and Stiffness at Follower	**3.301**	**1.66E+07**

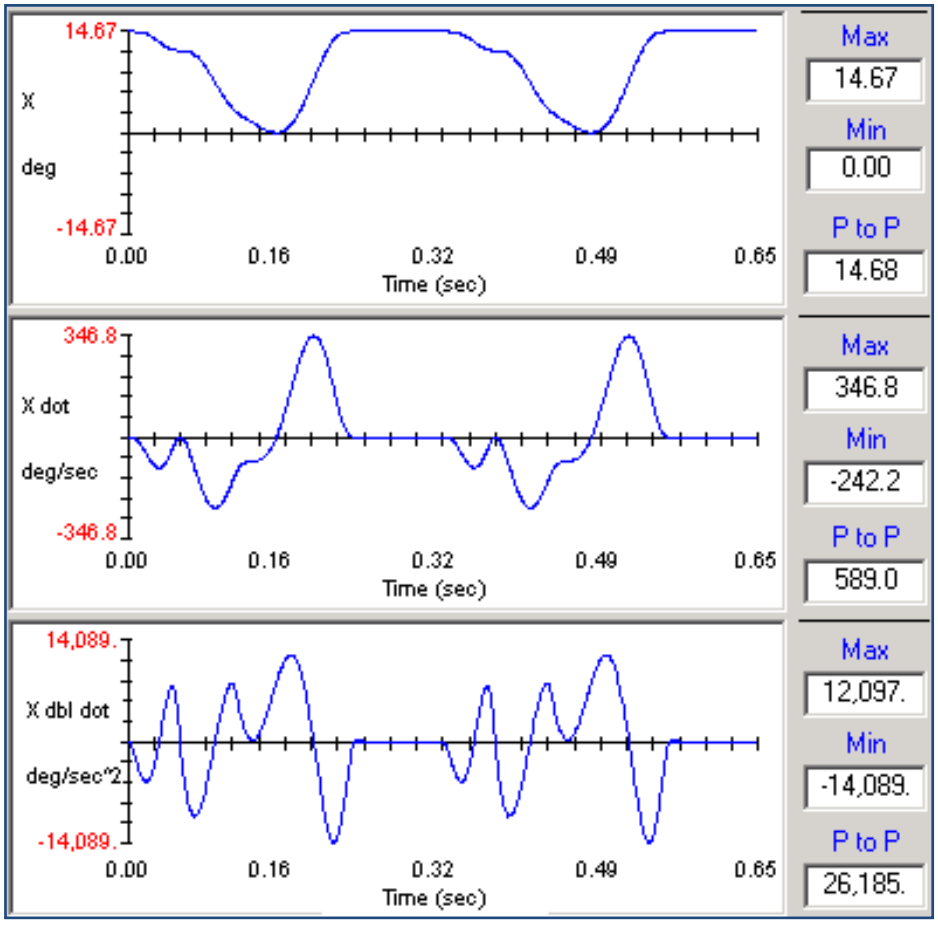

Figure 3.12: Inserter Vibration Simulation (two cycles shown)

4 Analysis

We performed an extensive analysis of the physical machine in order to validate our models and identify the root cause of the binding issue. Our investigation included testing the machine with accelerometers, filming machine operation with a high-speed camera, and inspecting parts under a microscope.

4.1 Accelerometer Testing

We gathered experimental data to verify the accuracy of the dynamic simulation and to determine the critical forces and moments acting on the system. This was done by recording accelerometer data on the actual machine and observing locations that exhibited high accelerations or impacts.

The equipment used to gather the data included three accelerometers and a signal analyzer. The accelerometers used were Dytran models 3056A2 and 3055B1. The 3056A2 (S/N 258) or 3055B1 (S/N 4333) model was used on channel one depending on the test and model 3056A2 (S/N 259) was used on channel two throughout testing. Accelerometers were placed on both bellcranks and on each hard stop, as shown in Figure 4.1. The data was collected using a Hewlett Packard model 35670A Dynamic Signal Analyzer.

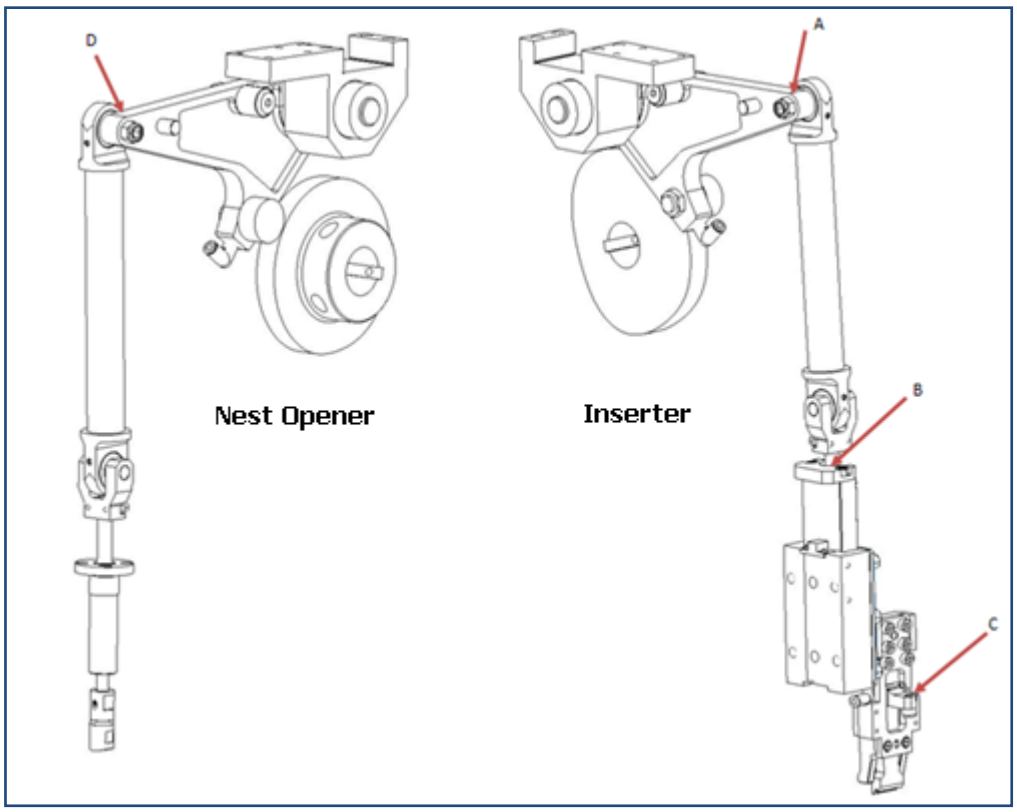

Figure 4.1: Nest Opener and Inserter accelerometer placements

There were six tests conducted with the accelerometers, though only five of the tests produced useable data. For all of the tests, the analyzer was set with enough lines to cover more than 1full cycle, with a Hanning window and a bandwidth capable of capturing the nuisances of the movement. The frequency bandwidth is locked to the time base with the relation $T = \frac{1}{F}$ where T is the period and F is frequency.

The trigger to start the collection of data was taken directly from the machine which ensured that all of the test data would have the same starting location with respect to the cam. After the trigger activated, about 1.5 machine cycles of data were recorded and then averaged. The two styles of data collected were time and linear spectrum for a total of four traces per test. Once the data were collected and saved, the trace files were converted and imported into Excel for analysis. A log of the tests can be found in Appendix C.

4.1.1 Graphs of Theoretical & Dynamic Motions with Experimental Data

We superimposed the experimental data with the kinematic and dynamic simulation data to compare the simulated and actual performance of the machine. Moreover, the degree to which the modeled and experimental data matched-up provided justification to use the models to analyze new designs.

To create these graphs we had to transform the experimental data to match the DYNACAM output. First, we had to ensure that the 'positive' direction of the accelerometers coincided with the modeled acceleration direction. We determined that vertical-up was the positive direction for all the test cases, which followed the simulated data; so no change had to be made to account for acceleration direction. Next, we had to center the experimental data about zero because the piezoelectric accelerometers give an inaccurate DC value. To do this we found the average of the experimental data set and subtracted it from all the values.

The accelerometers measured tangential acceleration, so to match the test data we converted the DYNACAM output from deg/sec^2 to g's of acceleration using the following relation:

$$A_g = \frac{\pi * r * \alpha}{180 * g}$$

Where $\boldsymbol{r}$ is the radius from the fixed pivot to the conrod pin (length $\boldsymbol{a}$ in Figure 3.11); $\boldsymbol{\alpha}$ is the rotational acceleration of the follower; and $\boldsymbol{g}$ is the gravitational acceleration constant.

Since the accelerometer was triggered at an arbitrary position in the machine cycle, we had to phase shift the data to line up properly with the DYNACAM output. Our approach was to phase-shift the experimental data by small degree increments until it satisfactorily phase-matched the DYNACAM output. We picked points on either data set that were essentially on the horizontal axis, kept the DYNACAM data stationary, and moved the experimental data back-and-forth until the functions lined up to within approximately ±1 degree.

We then observed the entirety of the experimental and simulation graphs to ensure they were suitably matched-up. One example of a combined graph that matched up well is shown in Figure 4.2. The match is evident because the shape of the functions and horizontal

location of major inflection points are all similar among the three plots shown. The reasonable correspondence between the DYNACAM output and experimental data validates using the models to analyze new design iterations.

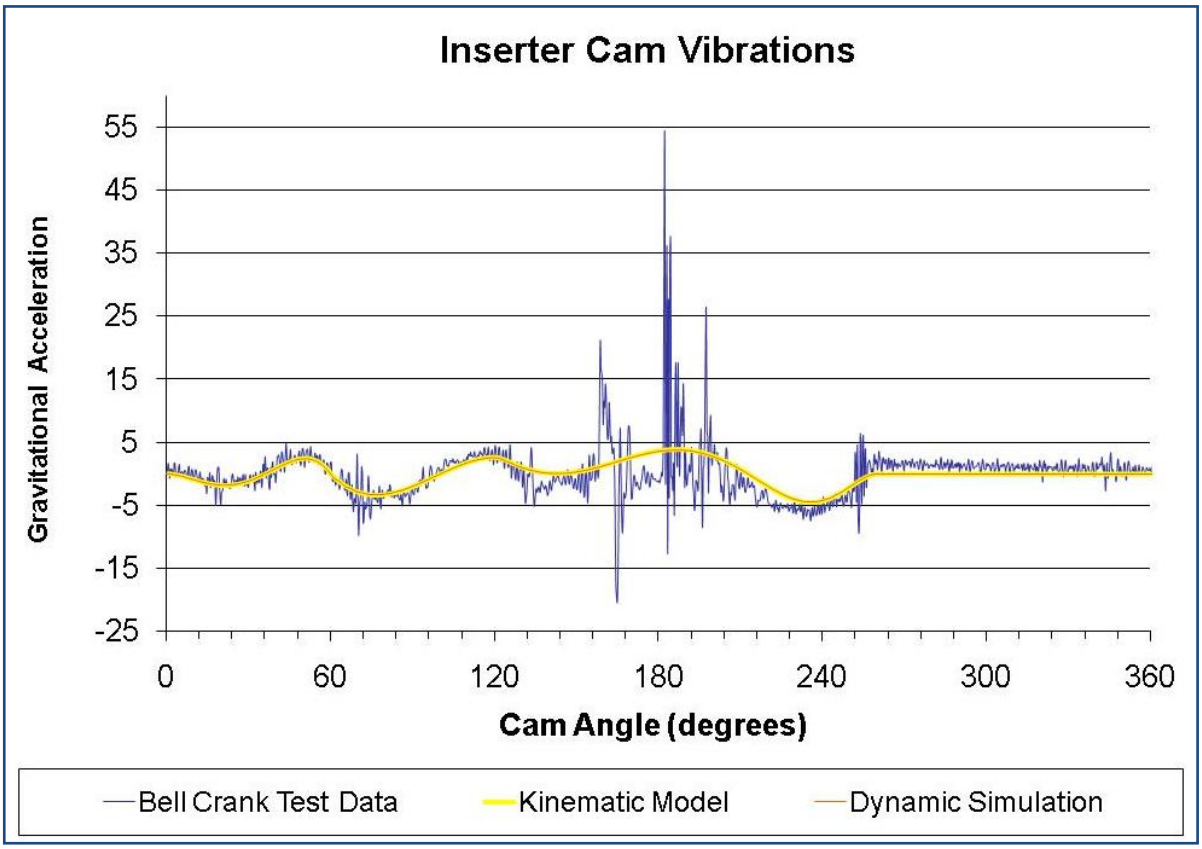

Figure 4.2: Inserter cam vibrations

A running average was taken to reduce the noise in the raw data in order to make comparisons with the simulations, as shown in Figure 4.3. The data revealed four distinct peaks due to impact. The point marked **A** is due to the vacuum head hitting its hard stop while **D** is the vacuum head being picked back up by the retracting slide. Peaks **B** and **C** are both due to the main slider hitting its hard stop then having the over travel spring absorb the impact.

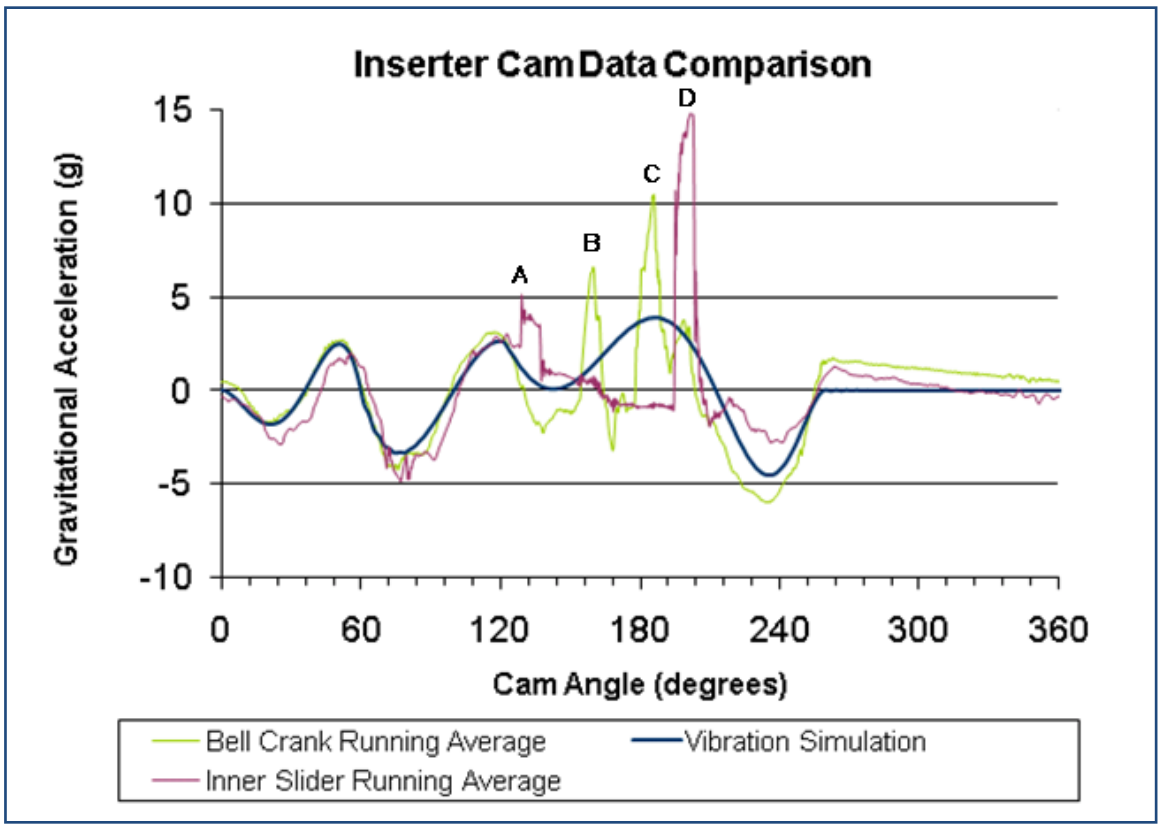

Figure 4.3: Inserter cam data comparison

Figure 4.4 shows the nest opener system experimental data compared to the dynamic simulation. It is clear that the data generally matches the simulation very closely. The one exception is the large peak near the middle of the cycle. This is due to the tappet accelerating away from the nest opener release button. Overall, the acceleration profile of the original nest opener system was fairly mild, and since this system did not directly contribute to the vacuum slide binding, we chose to discontinue our analysis of it.

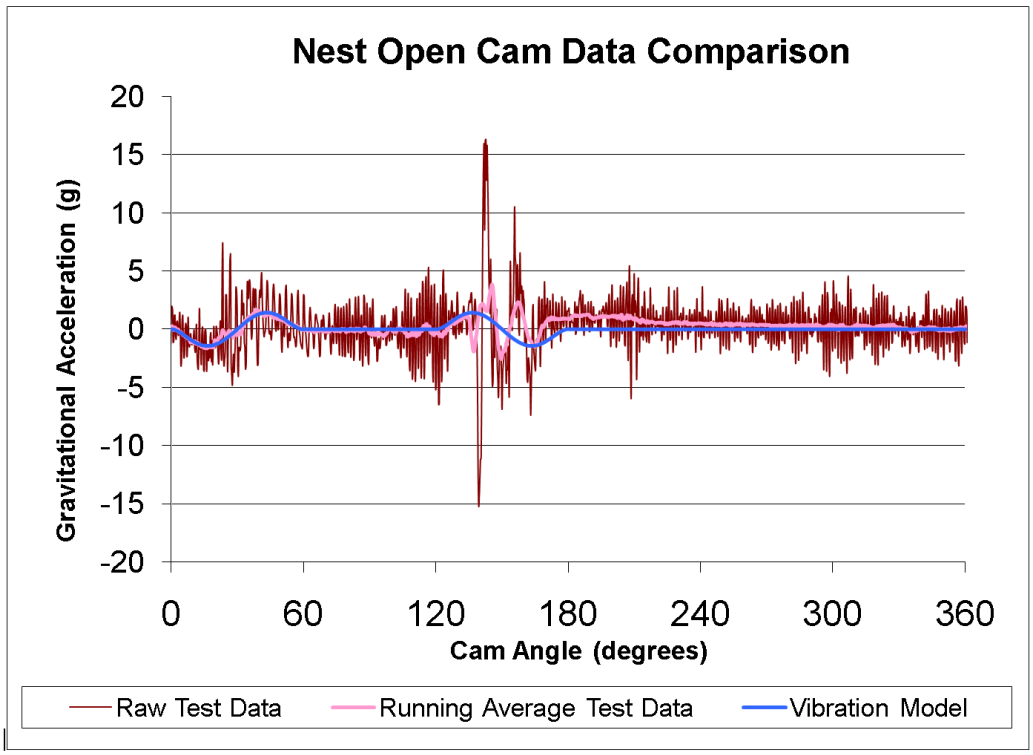

Figure 4.4: Nest Opener cam data comparison

4.2 High-Speed Video

Along with the accelerometer data, high-speed video of the mechanism was taken with the camera set up in different orientations. The camera was running at 1000 frames per second during all of the videos. The orientations included a view that showed the lower section of the inserter system, the motion of the top half of the mechanism, and a close up of the first hard stop that hits the rail.

The video of the lower section of the inserter system focuses on when the vacuum head picks up the product to fully seating the product in the container and then retracting to its starting position (see Figure 4.5). The footage was slowed then examined to observe the motions of the linkages when the machine is operating. When the vacuum gripper head reached its fully extended position, the vacuum head could be seen shaking slightly horizontally. This noticeable shaking was most likely caused by vibrations from the vacuum head stop impacting the stop rail, which we felt could be evidence that the impact was in some way related to the binding.

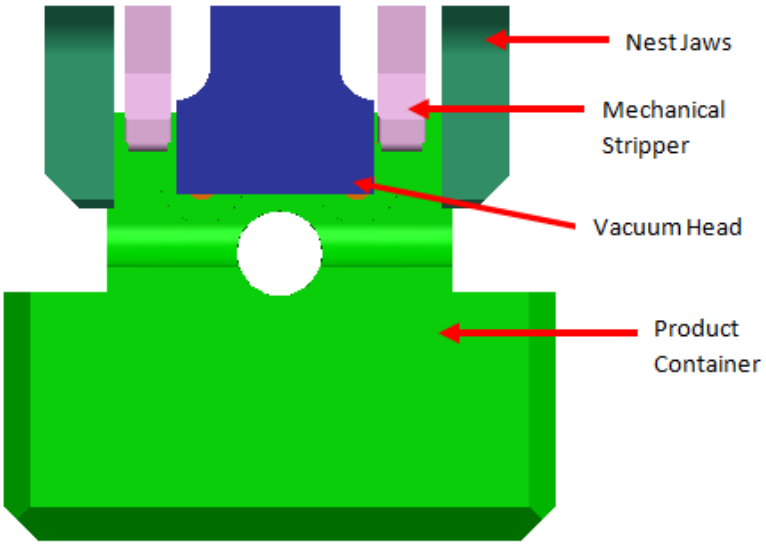

Figure 4.5: HSV view of product transfer from nest to container (product image removed)

The next view involved the back of the machine and showed the slider with the two hard stops which were marked to enhance their visibility in the video (see Figure 4.6). It appeared that the upper hard stop causes the lower stop to bounce while it is resting on the rail stop. We took another video that zoomed-in on the lower stop, but we could not confirm any jumping. Also, we were unable to find evidence of jumping in the accelerometer data. We concluded that the supposed jump was probably just a shadow in the footage.

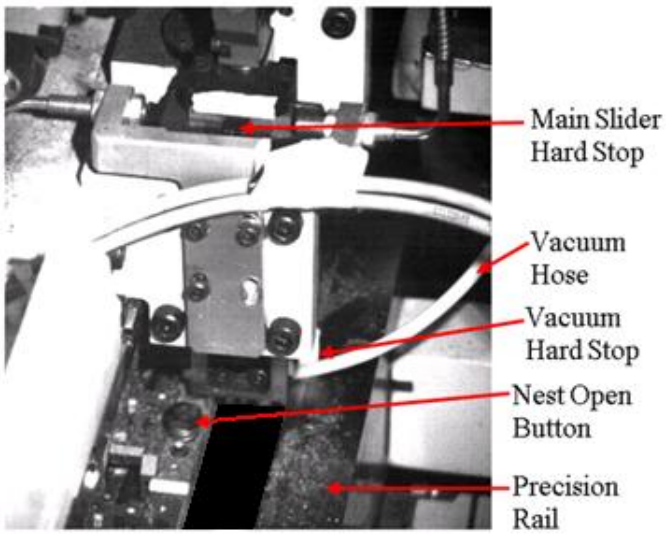

Figure 4.6: HSV view of two hard stops

4.3 Causes of Binding in the Slider Mechanism

After examining all of the data, it was determined that the best place to start looking for potential improvements would be in the inserter system. Once the problematic section was identified, more in-depth analysis was required to find probable causes for the binding. After discussing the binding issue with a few of the engineers, it was determined the binding was occurring in the smaller slider that houses the vacuum gripper and the mechanical strippers.

4.3.1 Wear

Beneath the inserter assembly, there was a buildup of residue on the stop rail that consisted of plastic, metal, hair and other materials. The residue was cleaned up and by the next day, more had accumulated. A sample of the residue was examined under a microscope and can be seen in Figure 4.7. We felt that the metal particles in the residue could point to excessive wear occurring within the vacuum slide assembly. We wanted to investigate the inserter assembly further to confirm the presence of excessive wear and determine its relation to the binding.

Figure 4.7: Enlarged Image of Residue

Examination of the slider components after disassembly revealed discrete sections of wear, as shown in Figure 4.8. We determined that these distinct wear marks were caused by

the repeated load applied from the slide as it rests on the stop rail. When the hard stop hit, it caused a moment that forced the edge of the vacuum head into the slider. We felt that this wear was directly related to and caused by the binding, so we needed to focus on the cause of this wear when developing design iterations.

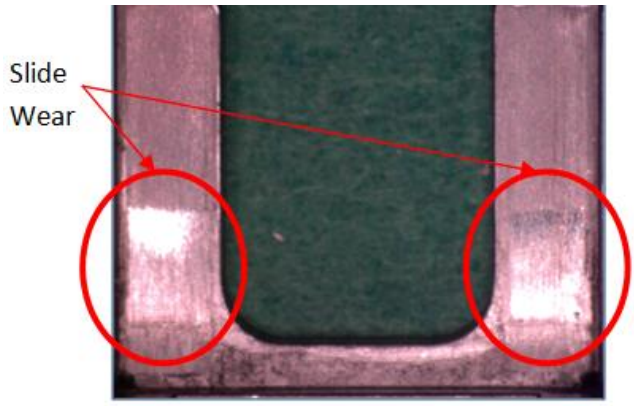

Figure 4.8: Vacuum slide wear caused by hard stop

We also noticed wear from maintenance workers stoning the surfaces to restore a good surface finish after they became scored. Stoning wear on the vacuum head slider can be seen in Figure 4.9. The stoning removed the coating on the parts, which meant that the friction between the surfaces was higher than it was designed to be. We hoped that by reducing the occurrence of binding, we would reduce the need to stone these sliding surfaces, which would help keep them sliding smoother longer.

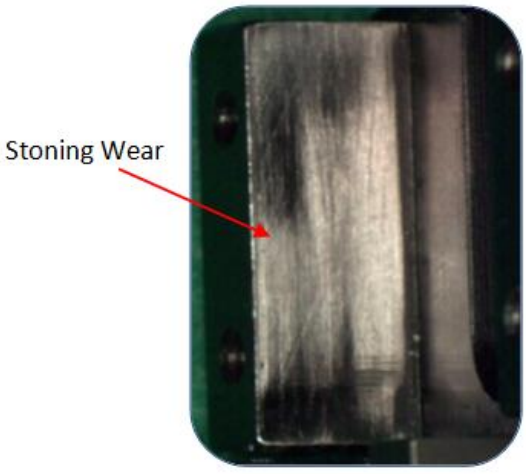

Figure 4.9: Vacuum slide wear caused by stoning

4.3.2 Bearing Ratio

Since we were investigating sliding parts, an important aspect to evaluate was their bearing ratios. The bearing ratio is the effective length over the effective diameter or in our case the instantaneous contact length of the slide over the width of the slider. For a bearing to operate effectively with little to no binding the bearing ratio should be at least 1, but preferably above 1.5.

The maximum bearing ratio of the vacuum head slider is 0.719 and the minimum bearing ratio for the slider when fully extended is 0.438. The minimum bearing ratio for the main slider was 2.5. After comparing the two sliders, we determined that the bearing ratio of main slider was quite sufficient, while the bearing ratio of the vacuum slide could definitely be improved. We felt strongly that the poor bearing ratio of the vacuum slide was a major cause of its binding.

4.3.3 Impact Forces and Applied Moments

The vacuum slider assembly experiences two hard stops during its motion. The first hard stop occurs when the stop on the vacuum head cap hits the precision rail on the adjacent conveyor. This hard stop prevents the vacuum head from inserting the product too deep into the product container. Also, it allows the insert and stuff motions to be driven by the same cam, as it holds the vacuum gripper in place while the strippers extend to strip and stuff the product into the container. The second hard stop prevents the mechanical strippers from over-travelling into the product containers and breaking the product and/or the container.

The impact zones for both the main slider and vacuum slide were cantilevered from the parts to allow them to hit their stops without interfering with adjacent components. The main slide body had a very short cantilever, so only a small moment was applied during its impact. Moreover, the magnitude of the impact was relatively small because the slide body was traveling at low velocity as it hit.

Raw accelerometer data showed a 170g spike during the hard stop impact. This impact applied a significant moment due to the relatively long moment arm of the cantilevered vacuum head stop, as illustrated in Figure 4.10. These observations indicated

that this impact was closely related to the binding and was responsible for the excessive wear observed on the slide. Combined with the effects of the poor bearing ratio, we decided that the vacuum slider components would be the main focus of our redesign.

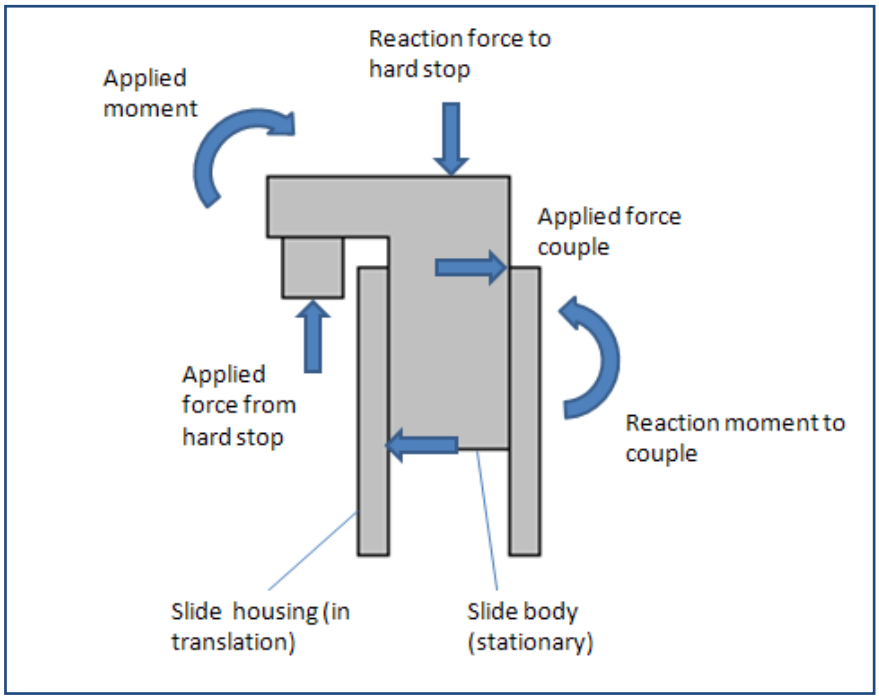

Figure 4.10: FBD of vacuum slider at hard stop impact

5 Redesign

The proposed redesigns included modifying several components of the inserter system in order to reduce the chance of it binding. These changes can be grouped into two separate categories, the product inserter assembly components and the cams.

Major considerations for the inserter assembly redesign were improving the vacuum slide's bearing ratio and reducing the moments caused by its hard stop. The redesigned components were then analyzed to determine changes in effective mass and stiffness. Concurrently, the inserter cam was modified to reduce velocity at impact to reduce the magnitude of the impact force on the vacuum slide hard stop. For each of the cam design iterations, we compared motion and dynamic force profiles and evaluated cam-follower separation and wear characteristics. Although the following explains our final design, information about an initial solution we developed is described in Appendix D.

5.1 Vacuum Head Slide Components

To ensure smooth operation, sliding components should have a minimum bearing ratio of at least 1.5. The original bearing ratio had maximum and minimum values of 0.72 and 0.48, respectively. The proposed design has a bearing ratio with a minimum ratio of 1.6. The increase in the bearing ratio was a result of lengthening the vacuum head and corresponding slider housing while decreasing the width of the vacuum head as seen in Figure 5.1. To achieve the improved bearing ratio, the slide housing and gibs also had to be modified. These changes also required the assembly to be moved up to accommodate the extra length of the slider.

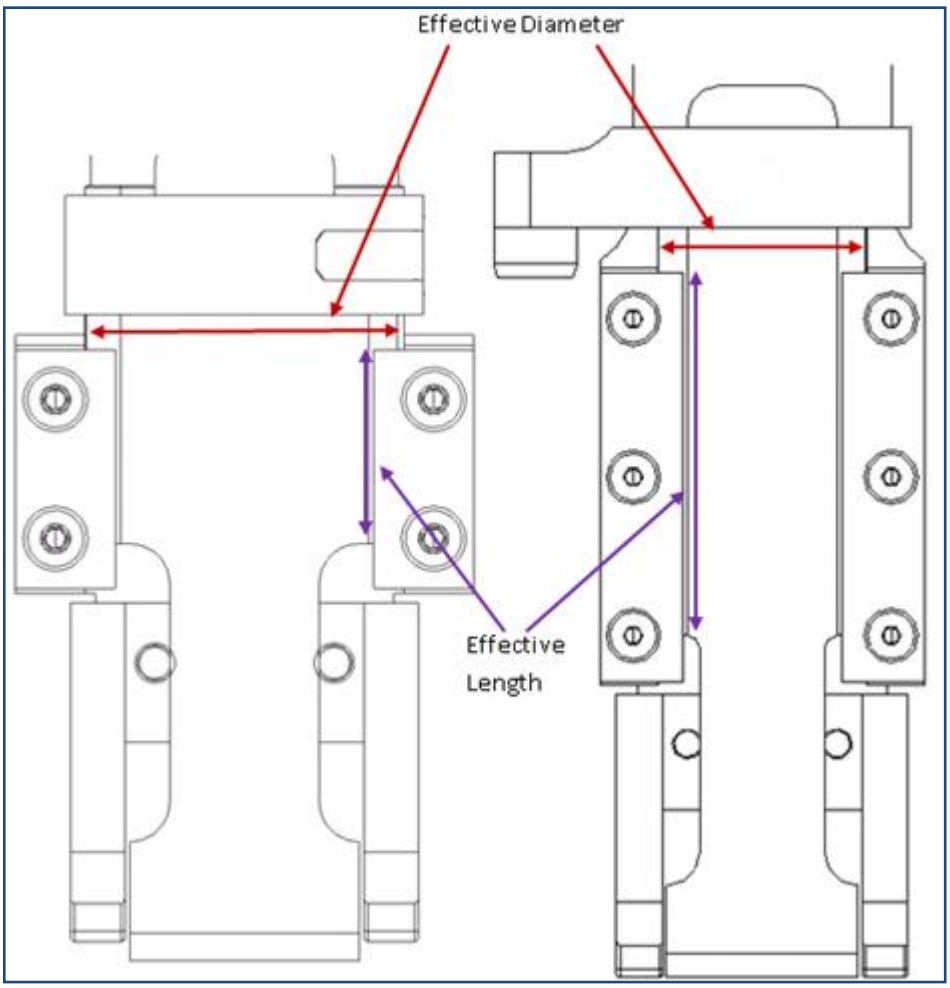

Figure 5.1: a) Original Vacuum Head b) Redesigned Vacuum Head

5.1.1 Vacuum Head Hard Stop

The hard stop was redesigned to accommodate the modifications made to the slider as well as to reduce the moments applied by the impact. The existing design of the stop of the vacuum head consisted of an air hose valve on the side and the hard stop on the back. The single hard stop created a moment since it was located on a cantilever.

The redesigned stop can be seen in Figure 5.2 and the cap on the vacuum head can be seen in Figure 5.2. This design has one hard stop to the side and the air valve in the front. The benefit of the new position of the stop is that the impact causes a moment around a stiffer axis; and with the longer slide, the force of the couple applied to the sliding surfaces is nearly 45% less than the existing design.

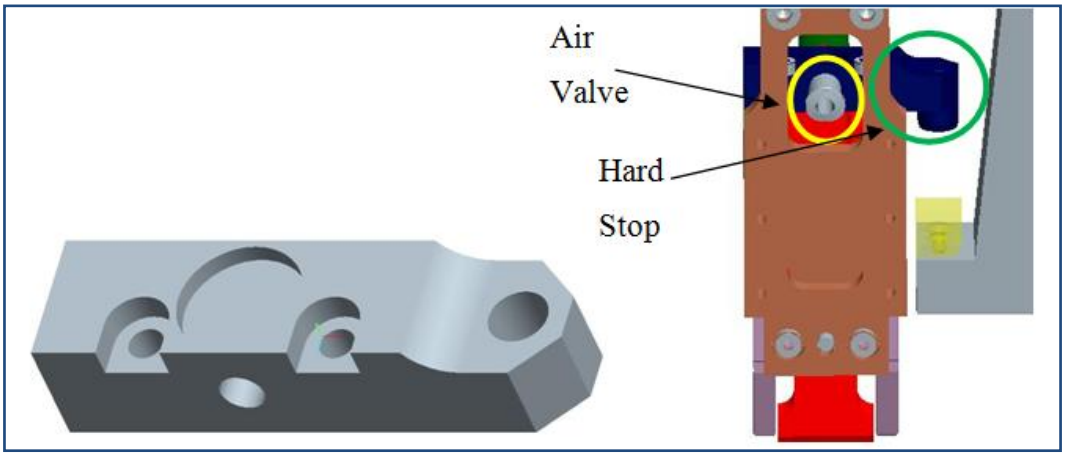

Figure 5.2: New Vacuum Head Stop and Vacuum Assembly

The major premise of the vacuum head stop redesign was to move to a single hard stop located on the side of the assembly, in order to maintain visibility and access to nearby components. The improved design incorporated a hard stop to the side of the weldment, as shown in Figure 5.2. This new feature included a small wear pad that can be ground to a specific height or replaced after significant wear compromises its functionality. Although it does not eliminate the overturning moment applied by the impact, it allows for an improved bearing ratio during the impact.

Aside from the weldment modification, we decided to improve the way in which we moved the assembly up to accommodate the longer slide. The first redesign included a goose-neck style slider mounting bracket that decreased the effective stiffness of the system. The new redesign moves the assembly up by shortening the connecting rod. This maintains the original vacuum sub-assembly mounting bracket and actually improves the overall stiffness of the system.

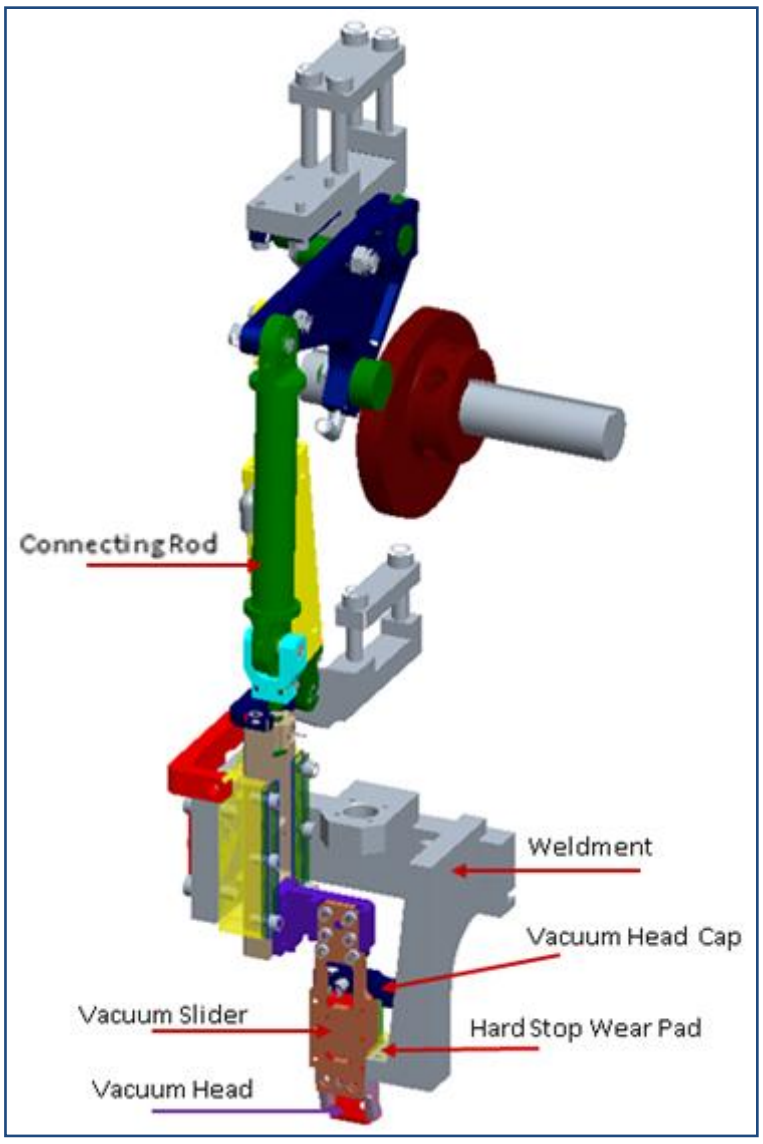

Figure 5.3: Final redesign

5.2 Slider Component Redesign Validation

The largest change in the new design is the modification of the weldment. However, all of the parts in the redesign had to meet the existing maximum deflection limits and have an infinite life. Since there were only two parts that were drastically redesigned, only the new vacuum head and the weldment needed to be validated.

The critical force applied to these two components was the force of impact as the vacuum head travels downward. Although a few different force estimates can be made, the

impact force could not be determined with high confidence. This led to reverse engineering the existing vacuum head to determine what impact force would cause it to fail to meet infinite life. Since we know it has not failed, the impact force must be less than that value. The impact force to fail the part in fatigue was determined to be close to 1kN. This is the largest force needed to evaluate the safety of the new design. Both components were then checked using SolidWorks. The simulations were done as shown in the CAD modeling section of this report. The simulation was run assuming: zero-based repeated stress, Gerber method for the mean stress correction, and von Mises equivalent stress. The Gerber method is not the least conservative approach; however it is the most accurate.

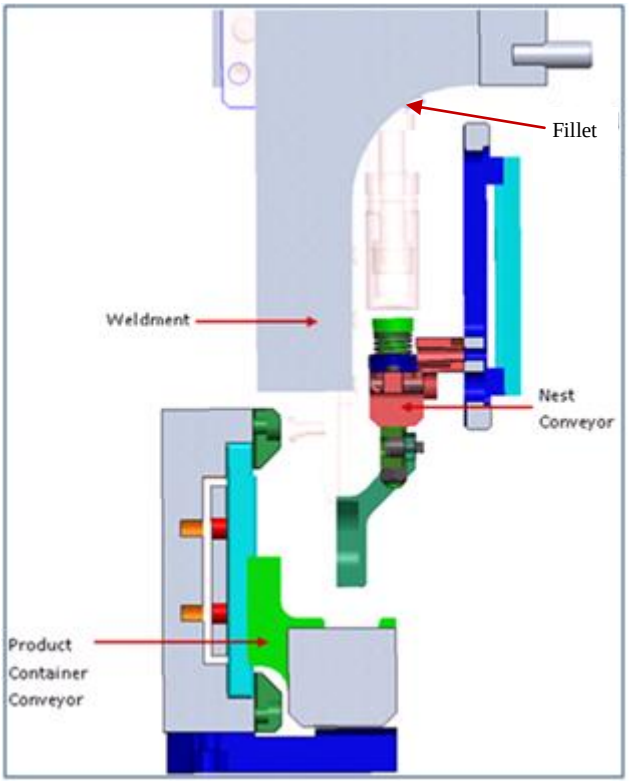

Figure 5.4: Weldment side view

The vacuum head stop and the right arm of the weldment designs were iterated to withstand the force of the hard stop. The general design modifications were to stiffen the cantilever section without impeding any other motions of the existing system. Instead of a rectangular beam, the supporting arm is tapered to be thicker at the bottom for strength.

There is a fillet on the right arm which allows for the nest conveyor to move past it without interference, as shown in Figure 5.4. The fully modified weldment is shown in Figure 5.5.

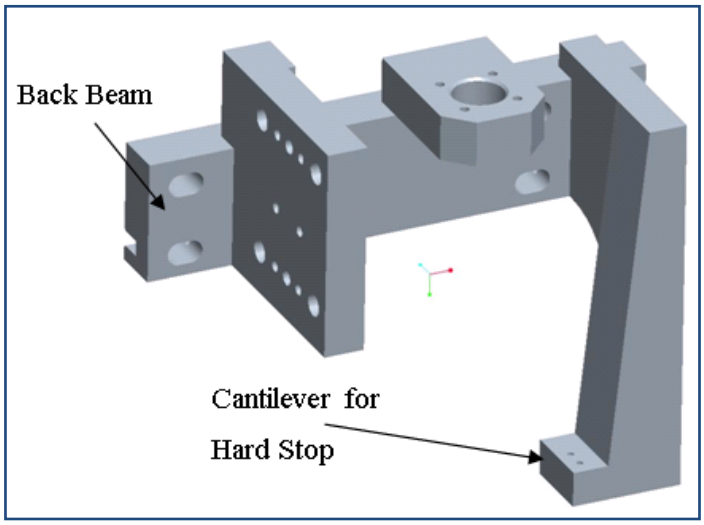

Figure 5.5: Final Weldment design

The model of the redesigned slider assembly was analyzed to evaluate changes to effective mass and stiffness. Table 5.1 summarizes the results of this study. The effective mass of the system increased 4.4%, but we feel this will not have any negative effect because the components are still fairly light-weight. The effective stiffness decreased 10.7%, but we do not foresee any issue with this because the existing system was very stiff to start with and even with this decreased stiffness, the vibrations will still be minimal.

Table 5.1: Changes in effective mass and stiffness

	Effective Mass (kg)	Effective Stiffness (MN/m)
Existing	7.419	18.7
Proposed	7.749	16.7
Change	4.40%	-10.70%

5.3 Cam Redesign

The focus of the cam redesign was to reduce the velocity at the vacuum head impact in order to reduce the impact force and consequently decrease the amount of wear on the sliding surfaces. A secondary focus was to reduce the average dynamic force over the machine cycle so that the existing cam wear characteristics are maintained. However, we made sure to check that our new dynamic force profile would not cause follower jump.

Several sets of functions were looked at to find the best design for the cam. Each of these sets included a dwell. With the follower train's complex motion, simple functions such as modified sine, trapezoid, and cycloid were not suitable. Instead, B-splines were used because they allow for greater control of functions with many boundary conditions.

To control the spline functions three methods were used. First, boundary conditions were entered into DYNACAM so the function would go through all the critical points and there would be no discontinuities between the functions. A spline order of seven was chosen that provided nineteen knots. These knots were positioned to provide reasonable numbers for displacement, velocity, acceleration, and jerk. Figure 5.6 shows the boundary condition and knot control screens for our new inserter cam design. A discontinuity check, as shown in Figure 5.7, was performed to ensure smooth cam motion throughout the machine cycle. The check showed that the cam functions were continuous through jerk.

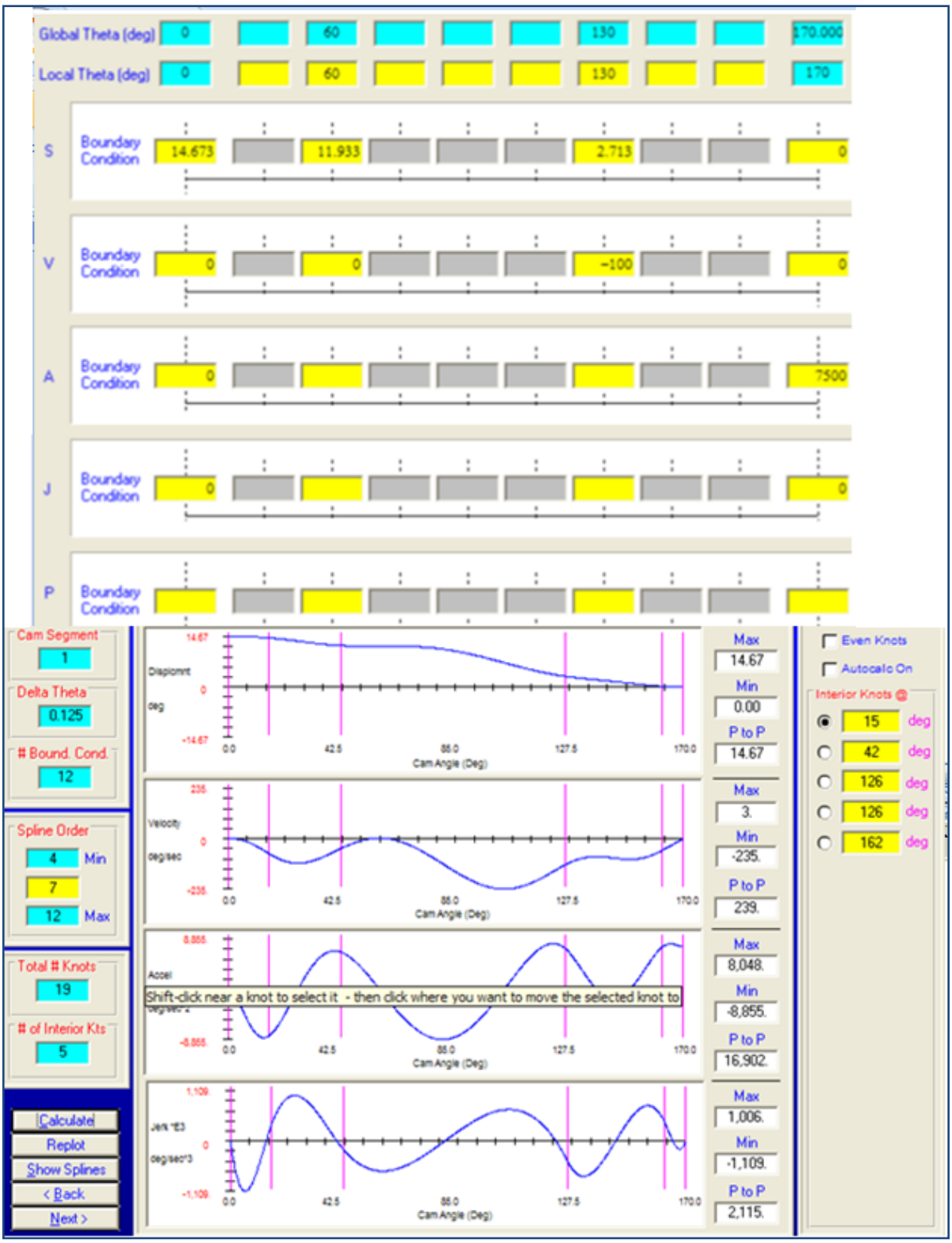

Figure 5.6: Boundary conditions and knot control screens

Resulting Boundary Values at Segment Interfaces

Segment	End	S	V	A	J
1	1	14.673	0	-0.081	0.021
1	2	0	0	7500	0
2	1	0	0	7500	0
2	2	14.673	0	0.182	-0.051
3	1	14.673	0	0	0
3	2	14.673	0	0	0
1	1	14.673	0	-0.081	0.021

Figure 5.7: Discontinuity check

The resulting new cam's rise-fall segment was lengthened 10 degrees, as shown in Figure 5.8, to account for the reduced velocity within it. A comparison of the existing and proposed cam designs shows a 34% reduction in velocity at the vacuum head hard stop, as shown in Figure 5.9. The two hard stops are shown in their approximate locations as dotted vertical lines.

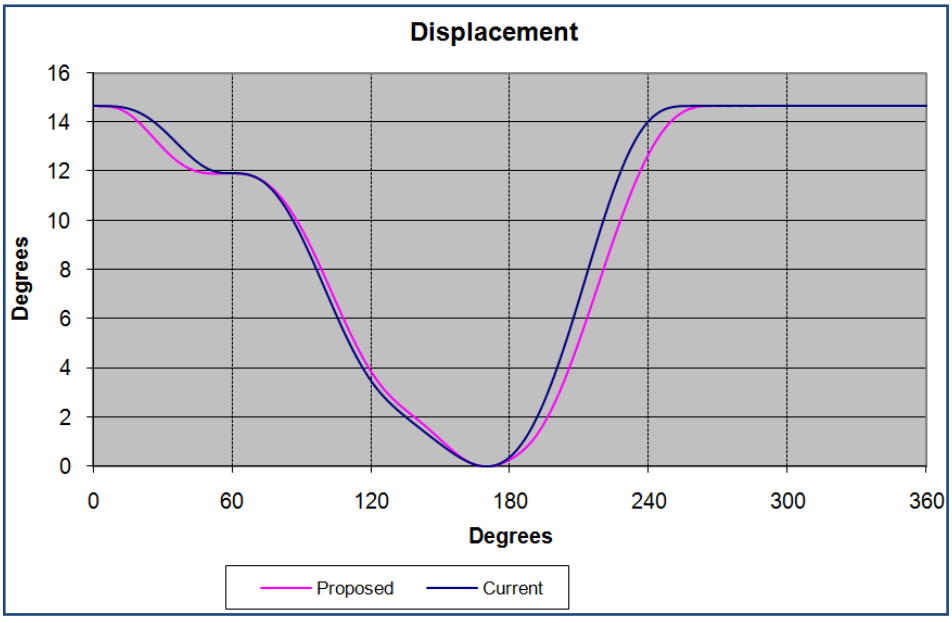

Figure 5.8: Cam displacement comparison

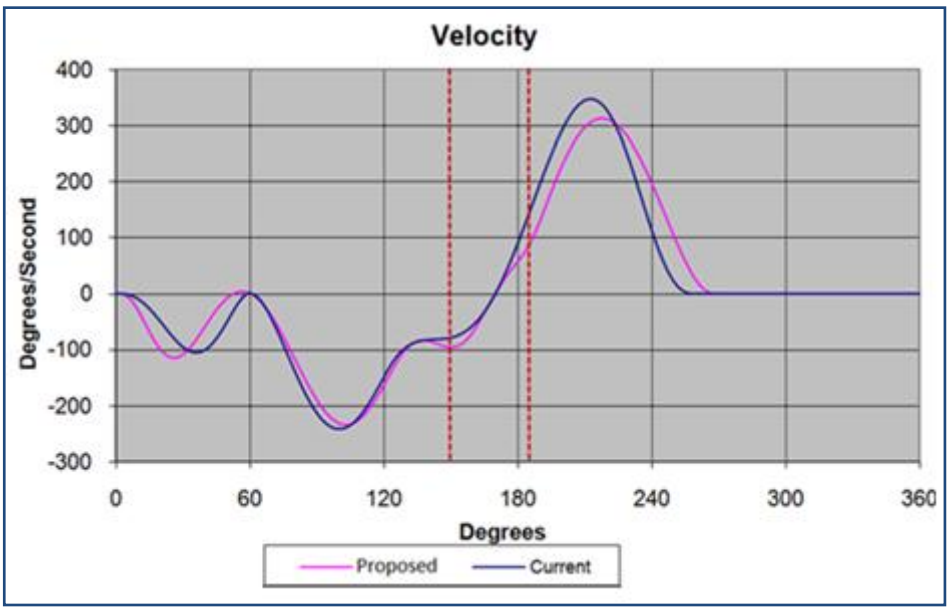

Figure 5.9: Cam velocity comparison

5.4 Testing of New Cam

We were able to manufacture a prototype of this cam and test it on the machine to evaluate the effects reducing the velocity had to the magnitude of the impact force at the vacuum slider hard stop. The setup and protocol followed that which was described in the Analysis section.

Initial tests were run using the existing cam in order to verify that the data matched what we obtained from the original analysis. Then, the new cam was installed and more acceleration data was taken. We ran several tests with this cam to ensure that we obtained accurate data.

The test data was matched up to the proposed cam's vibration simulation the same manner described in the Analysis section for the existing cam. Figure 5.10 shows that the data matched up very closely, which gave us confidence to trust the results of both simulation and machine analyses. The peak acceleration, which occurred during the vacuum slider hard stop, showed a 17% reduction, as depicted in Figure 5.11. Furthermore, the RMS acceleration decreased 4.6%. This results in lower dynamic forces, which would eventually lead to less wear on the sliding components, as well as on the cam.

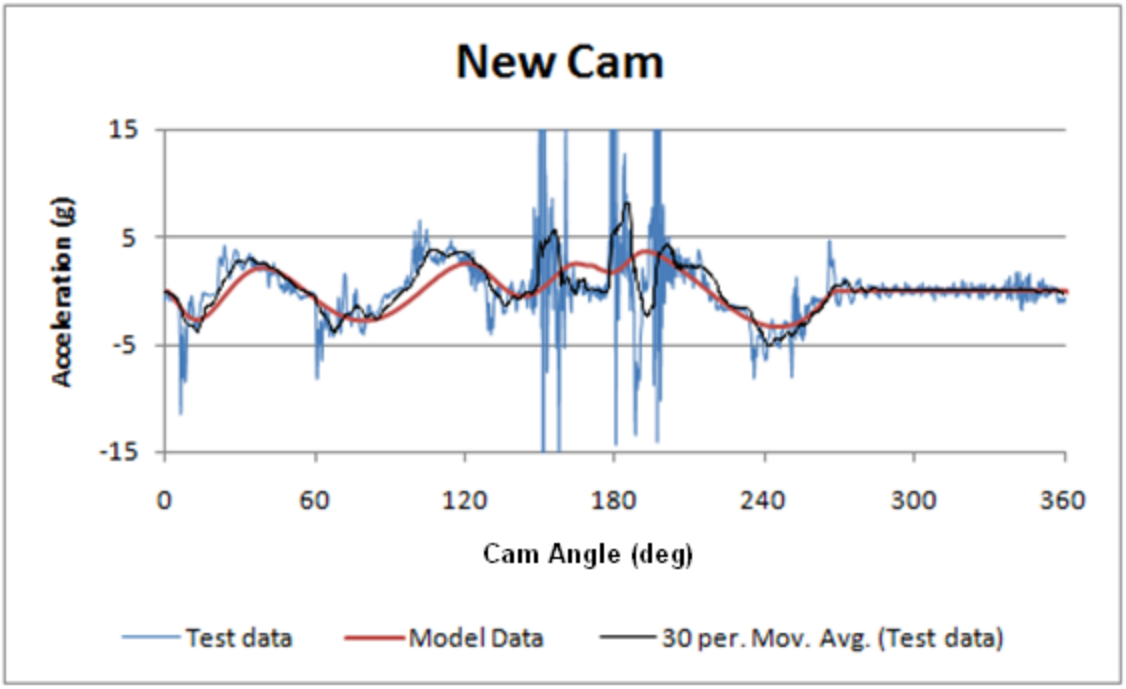

Figure 5.10: New Inserter cam test data compared with simulation

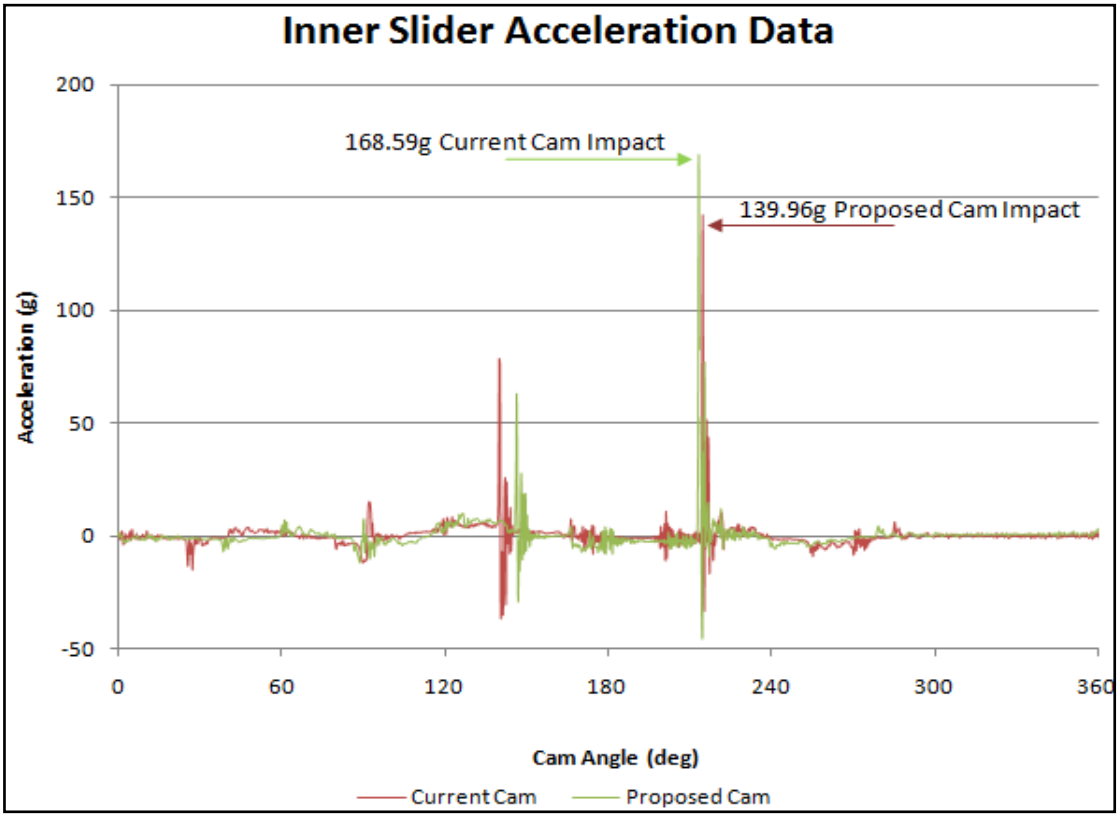

Figure 5.11: Test data for current and proposed cams

6 Conclusions and Recommendations

During our residency at the sponsor's company, we indentified the root cause of the problem and developed a feasible solution to address the binding problem with the product inserter mechanism. Our design was achieved through accurate modeling and careful analysis of the existing system and of new design iterations. We created models using CAD software and developed dynamic simulations using DYNACAM. These models were verified by comparing them to physical measurements and observations via accelerometer tests, high-speed video footage, and inspection of parts under a microscope. We obtained very good matching between test and model data, so we were confident that we could use our simulations to predict changes within the system due to newly designed components.

To eliminate the binding, we redesigned the vacuum slider assembly to have a minimum bearing ratio of 1.6, which is a significant improvement over the existing 0.72 maximum bearing ratio. This improvement was achieved by making the slide and mating components longer and narrower. We had to accommodate for the longer slide in order to maintain the existing precision positions of the tooling. This was done by shortening the connecting rod and shifting up the mounting holes for the main slider assembly (so as not to disturb the large bearing ratio it presently had). The new assembly was effectively 4.4% more massive and 10.7% less stiff, but since the existing assembly was already fairly light and very stiff, these changes were seen as minor tradeoffs.

The vacuum head stop was modified to reduce the effect of the applied moment on the slide assembly during the hard stop. The stop was relocated so that when the impact occurred, the moment was applied about a stiffer axis. A ledge was created on the side of the new weldment to serve as the anvil for the new hard stop. The advantages to this new weldment feature are that it moves the stop anvil on to the same sub-assembly and provides a means to strike a replaceable wear pad instead of a practically irremovable piece of framework. It also allows for a partial bench setup before final assembly of the station.

While the slider redesign directly addressed the incidence of the binding, we also redesigned the inserts assembly's cam to try and reduce the impact forces felt during the hard stop. This was achieved by reducing the impact velocity by 34%. We manufactured the

cam, tested it, and saw a 17% reduction in peak acceleration, which roughly corresponds to that much decrease in impact force. Moreover, the proposed cam reduced RMS dynamic forces by 4.6%.

We recommend that the sponsor implement the full redesign package we have presented because each section of the improved design has distinct benefits. Permanently implementing the new cam alone would reduce the premature wear currently being observed on the machine, but it would have no effect on the frequency of the binding. Conversely, implementing the new slider components alone will eliminate the binding issue and make setting up the station easier, but the impact forces could still cause excessive wear to the sliders. We strongly encourage the sponsor to implement both parts of the redesign because applying the full package will make the station run more reliably with less unplanned downtime and maintenance requirements.

7 Bibliography

Text References

Lipson, Charles. *Handbook of Mechanical Wear: Frettage, Pitting, Cavitation, Corrosion*; Ann Arbor, University of Michigan Press © 1961

Norton, Robert L. *Cam Design and Manufacturing Handbook*; Industrial Press, Inc. © 2002

Norton, Robert L. *Design of Machinery: An Introduction to the Synthesis and Analysis of Mechanisms and Machines*; Fourth Edition. McGraw-Hill Companies, Inc. © 2008

Norton, Robert L. *Machine Design: An Integrated Approach; Third Edition*. Pearson Prentice Hall Pearson Education Inc. © 2006

Computer Software

Dessault Systèmes. *SolidWorks Education Edition SP 4.0* © 2008

Microsoft Corporation. *Microsoft Office Excel 2007*. © 2006

Microsoft Corporation. *Microsoft Office Word 2007.* © 2006

Norton Associates. *DYNACAM PLUS Release 9 Rev 8.6.* © 2008

Parametric Technology Corporation. *MathCAD 14*. © 2008

Parametric Technology Corporation. *Pro Engineer Wildfire 4.0*. © 2008

8 Appendices

8.1 Appendix A – Masses and Stiffnesses of System Components

Initail System

Component	Displacement in Meters	Force in Newtons	value (N/m	Mass (kg)	Meff (kg)	Keff (N/m)	%M(n/o)	%K (n/o)
lever_cam_follower	5.3830E-05	500	9.289E+06	1.765935	6.832	18710000	100	100
slider1_asm	5.5610E-05	500	8.991E+06	0.892471				
37505MK_assym_asm	7.9320E-07	500	6.304E+08	0.144716				
Slider (vacuum head)	6.6580E-06	500	7.510E+07	0.155742				
pushrod_asm	4.0280E-06	500	1.241E+08	0.200517				
tarpet	5.7640E-07	500	8.675E+08	0.042993				
air_spring_rod	4.4970E-06	500	1.112E+08	1.69413				

Redesign 1 - all steel

Component	Displacement in Meters	Force in Newtons	value (N/m	Mass (Kg)	Meff (kg)	Keff (N/m)	%M(n/o)	%K (n/o)
slider1_asm	5.5610E-05	500	8.991E+06	0.979298	7.355	16990000	107.6552	90.80706
Slider (vacuum head)	6.6580E-06	500	7.510E+07	0.199355				

Redesign 1.1 - Al arm

Component	Displacement in Meters	Force in Newtons	value (N/m	Mass (Kg)	Meff (kg)	Keff (N/m)	%M(n/o)	%K (n/o)
slider1_asm	1.1460E-04	500	4.363E+06	0.860767	6.881	11320000	100.7172	60.50241
Slider (vacuum head)	6.6580E-06	500	7.510E+07	0.199355				

Redesign 1.2 - Al arm, more solid slider

Component	Displacement in Meters	Force in Newtons	value (N/m	Mass (Kg)	Meff (kg)	Keff (N/m)	%M(n/o)	%K (n/o)
slider1_asm	2.4470E-04	500	2.043E+06	0.852	6.846	6518000	100.2049	34.83699
Slider (vacuum head)	6.6580E-06	500	7.510E+07	0.199355				

Redesign 2.0 shorter conrod

Component	Displacement in Meters	Force in Newtons	value (N/m	Mass (Kg)	Meff (kg)	Keff (N/m)	%M(n/o)	%K (n/o)
slider1_asm	5.0610E-05	500	9.879E+06	0.969932	7.255	16260000	106.1915	86.9054
Slider (vacuum head)	1.6910E-05	500	2.957E+07	0.183947				

Final - double check of numbers

Component	Displacement in Meters	Force in Newtons	value (N/m	Mass (Kg)	Meff (kg)	Keff (N/m)	%M(n/o)	%K (n/o)
lever_cam_follower	5.3830E-05	500	9.289E+06	1.765937	7.162	16710000	104.8302	89.31053
slider1_asm	5.0680E-05	500	9.866E+06	0.969932				
37505MK_assym_asm	7.9320E-07	500	6.304E+08	0.142411				
Slider (vacuum head)	1.3650E-05	500	3.663E+07	0.187177				
air_spring_rod	4.4970E-06	500	1.112E+08	0.160084				
Conrod	1.0000E+00	500	5.000E+02	0.379342				

8.2 Appendix B – MathCAD Files

Bearing Ratio Calculations

l is the effective length
d is the effective diameter
a is the minimum value
b is the maximum value

Initial System

$l_{1a} := 14mm$ $d_{1a} := 32mm$ $l_{1b} := 23mm$ $d_{1b} := 32mm$

$$\frac{l_{1a}}{d_{1a}} = 0.438 \qquad \frac{l_{1b}}{d_{1b}} = 0.719$$

New System

$l_{2a} := 40mm$ $d_{2a} := 25mm$ $l_{2b} := 49$ $d_{2b} := 25$

$$\frac{l_{2a}}{d_{2a}} = 1.6 \qquad \frac{l_{2b}}{d_{2b}} = 1.96$$

Conrod Stiffness Calculations

$R := 25.4mm$

$r := 22.1mm$

$E := 206.8GPa$

L is the length
R is the outer diameter
r is the inner diameter
E modulus of Elasticity
A is the cross sectional area

$A := \pi\left(R^2 - r^2\right)$

Conrod 220

$L := 172mm$

$k := A \cdot \frac{E}{L}$ $\quad k = 5.921 \times 10^8 \cdot \frac{N}{m}$

Conrod 235

$L := 187mm$

$k := A \cdot \frac{E}{L}$ $\quad k = 5.446 \times 10^8 \cdot \frac{N}{m}$

Conrod 220 Redesign

$L := 141mm$

$k := A \cdot \frac{E}{L}$ $\quad k = 7.223 \times 10^8 \cdot \frac{N}{m}$

Equivalent Mass and Stiffness Calculations

System Lengths	System Masses	System Stiffness
$l_{conrod} := 180mm$	$m_{airrod} := .160084kg$	$k_{airrod} := 1.112 10^{8} \frac{N}{m}$
$l_{follower} := 90mm$	$m_{follower} := 1.765937kg$	$k_{follower} := 9.289 10^{6} \frac{N}{m}$
$l_{airrod} := 145mm$		
$l_{cm} := 45.2666mm$		

Cam Follower Train 37998BYG

Local Masses	Local Stiffness
$m_{conrod} := .417886kg$	$k_{conrod} := 5.446 10^{8} \frac{N}{m}$
$m_{tarpet} := 0.042993kg$	$k_{tarpet} := 8.675 10^{8} \frac{N}{m}$
$m_{pushrod} := .200517kg$	$k_{pushrod} := 1.241 10^{8} \frac{N}{m}$
	$k_{springh} := 8230.96 \frac{N}{mm}$

M Equivalent

$$m_{workh} := m_{tarpet} + m_{pushrod} + m_{conrod}$$

$$m_{eqh} := m_{workh} \cdot \left(\frac{l_{conrod}}{l_{follower}} \right)^2 + m_{follower} \cdot \left(\frac{l_{cm}}{l_{follower}} \right)^2$$

K Equivalent

$$k_h := k_{tarpet} \cdot k_{pushrod} \cdot k_{conrod} \cdot k_{follower} \cdot k_{springh}$$

$$k_{workh} := \frac{k_h}{\frac{k_h}{k_{tarpet}} + \frac{k_h}{k_{pushrod}} + \frac{k_h}{k_{conrod}} + \frac{k_h}{k_{follower}} + \frac{k_h}{k_{springh}}}$$

$$k_{eqh} := \left(\frac{1}{l_{follower}^{2}} \right) \left(k_{workh} \cdot l_{conrod}^{2} \right)$$

Cam Follower Train 37998BYH

Local Masses

$m_{conrod} := .379342\,kg$

$m_{vacuum} := .187177\,kg$

$m_{slider} := .969932\,kg$

$m_{37505mk} := .142411\,kg$

Local Stiffness

$k_{conrod} := 6.83510^{8}\,\frac{N}{m}$

$k_{vacuum} := 3.66310^{7}\,\frac{N}{m}$

$k_{slider} := .986610^{7}\,\frac{N}{m}$

$k_{37505mk} := 6.30410^{8}\,\frac{N}{m}$

$k_{spring1} := 2479.796\,\frac{N}{mm}$

$k_{spring2} := 51.012\,\frac{N}{mm}$

M Equivalent

$$m_{workg} := m_{vacuum} + m_{slider} + m_{37505mk} + m_{conrod}$$

$$m_{eqg} := m_{workg} \cdot \left(\frac{l_{conrod}}{l_{follower}} \right)^2 + m_{follower} \cdot \left(\frac{l_{cm}}{l_{follower}} \right)^2$$

K Equivalent

$$k_g := k_{vacuum} \cdot k_{slider} \cdot k_{37505mk} \cdot k_{follower} \cdot k_{conrod}$$

$$k_{workg} := \frac{k_g}{\left(\frac{k_g}{k_{vacuum}} + \frac{k_g}{k_{slider}} + \frac{k_g}{k_{37505mk}} + \frac{k_g}{k_{follower}} + \frac{k_g}{k_{conrod}} \right)}$$

$$k_{eqg} := \left(\frac{1}{l_{follower}^{\,2}} \right) \left(k_{workg} \cdot l_{conrod}^{\,2} \right)$$

K of Air Cylinder

$A_b := 466.277mm^2$

$A_c := A_b + 56.2920mm^2$

$P_o := 80psi$ $P_{atm} := 1atm$

$l_c := 62.5mn$

$x := 10mn$ Stroke

$P_o = 0.552\frac{N}{mm^2}$

$v_c := l_c \cdot A_c$

$k_{cylinder} := \frac{A_c^{\,2} \cdot (P_o + P_{atm}) v_c}{(A_c \cdot x - v_c)^2}$

$F_{cylinder} := \frac{l_{airrod}}{l_{follower}} \cdot A_b \cdot P_o$

$k_{cylinder} = 7.737 \times 10^3 \cdot \frac{N}{m}$

System Values

37998BYH

$k_{eqh} = 1.665 \times 10^7 \cdot \frac{N}{m}$

$m_{eqh} = 3.092kg$

37998BYG

$k_{eqg} = 1.671 \times 10^7 \cdot \frac{N}{m}$

$m_{eqg} = 7.162kg$

Air Cylinder

$k_{cylinder} = 7.737 \times 10^3 \frac{kg}{s^2}$

$F_{cylinder} = 414.361N$

8.1 Appendix C – Accelerometer Test Data

Date 10/29/2008 Machine

STAT1.sta Machine
Setup Trigger Avg type

Accelerometer 1, 3 258, 4333
Transducer S/N Location
Ch 1

Accelerometer 2 259
Ch 2

Test#	Trace #	Chan	Msmt	BW	Lines	Wind	Avgs	Speed	unit	RMS value	unit	Peak value	unit	Comments
1	1	1	T	5S	800	Han	25		rpm					Acc on top of dog lever
	2	2	T	5S	800	Han	25		rpm					A1: 50g top
	3	1	LS	1.6khz	800	Han	25		rpm					A2: 50g top
	4	2	LS	1.6khz	800	Han	25		rpm					
2	5	1	T	5S	800	Han	25		rpm	DATA NOT GOOD				A3: 500g slider (slider)
	6	2	T	5S	800	Han	25		rpm					A2: 50g top
	7	1	LS	1.6khz	800	Han	25		rpm					
	8	2	LS	1.6khz	800	Han	25		rpm					
3	9	1	T	5S	800	Han	1		rpm					A3: 500g slider (slider)
	10	2	T	5S	800	Han	1		rpm					A2: 50g top
	11	1	LS	1.6khz	800	Han	1		rpm					
	12	2	LS	1.6khz	800	Han	1		rpm					A3: on vacuum head/ top of stop
4	13	1	T	5S	800	Han	25		rpm					A3: 500g slider (slider)
	14	2	T	5S	800	Han	25		rpm					A2: 50g top (further down; same system)
	15	1	LS	1.6khz	800	Han	25		rpm					
	16	2	LS	1.6khz	800	Han	25		rpm					A3: on top of slider housing
5	17	1	T	5S	800	Han	25		rpm					A3: 500g on rail (hardstop)
	18	2	T	5S	800	Han	25		rpm					A2: same as test 4
	19	1	LS	1.6khz	800	Han	25		rpm					
	20	2	LS	1.6khz	800	Han	25		rpm					
6	21	1	LS	3.2khz	800	Han	10		rpm					A3: same as test 5
	22	2	LS	3.2khz	800	Han	10		rpm					A2: same as test 5

8.2 Appendix D – Initial Design Iteration

In an initial concept of the insert redesign, the extra length of the new slide was to be absorbed by moving the slider housing upwards and redesigning its mounting bracket to account for the length increase. The old and redesigned brackets are shown below:

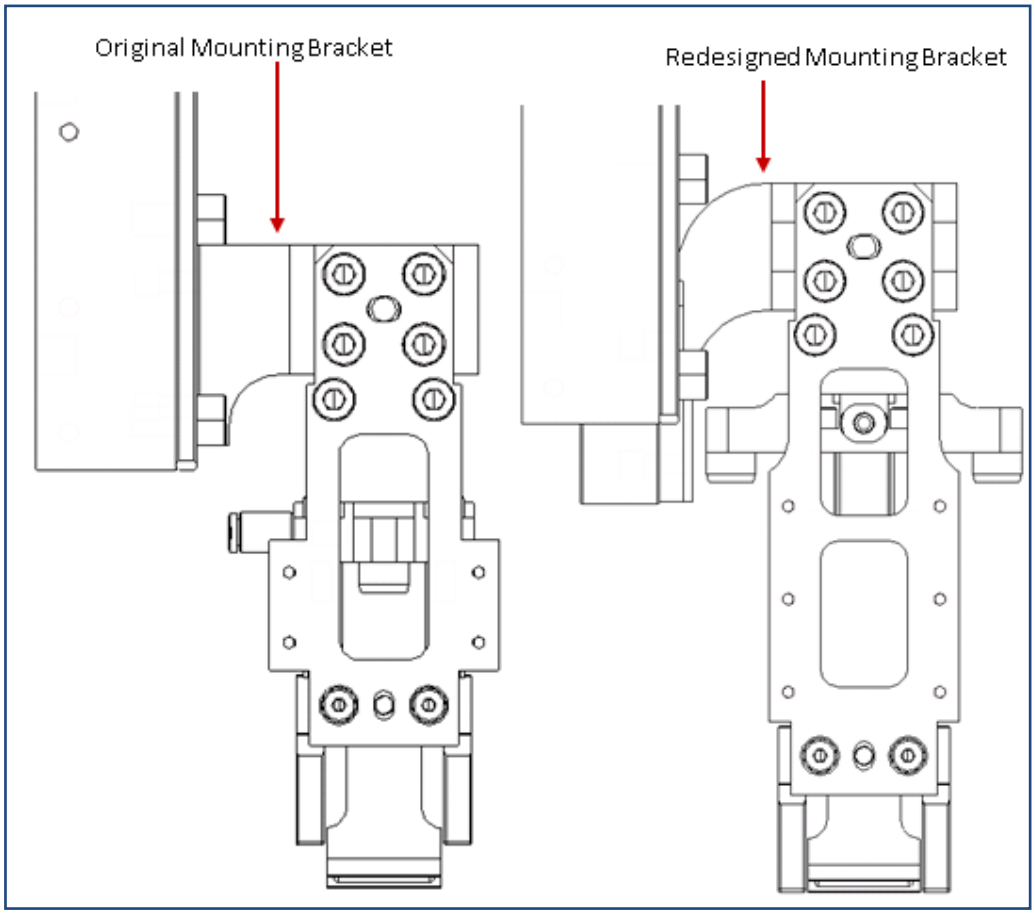

Mounting bracket comparison

The initial redesign removed the moment caused by the hard stop by changing the location of the valve and hard stop and adding a second hard stop to balance forces. The air valve has been moved to the back where the original hard stop had been located and the two hard stops are situated on the sides of the vacuum head stop. Also, the through holes for the screws that attach the vacuum head to the stop were moved in to match the new positions of the corresponding threaded holes on the vacuum head. The main advantage of this mirrored-stop design is that it cancels the moments applied by the hard stop impact.

The change in locations of the hard stop and air valve dictated a change in the arm connecting the vacuum head assembly to the rest of the inserter system. If the arm remained unchanged, there would be interference between the hard stop and the arm. The changes in the design are shown below:

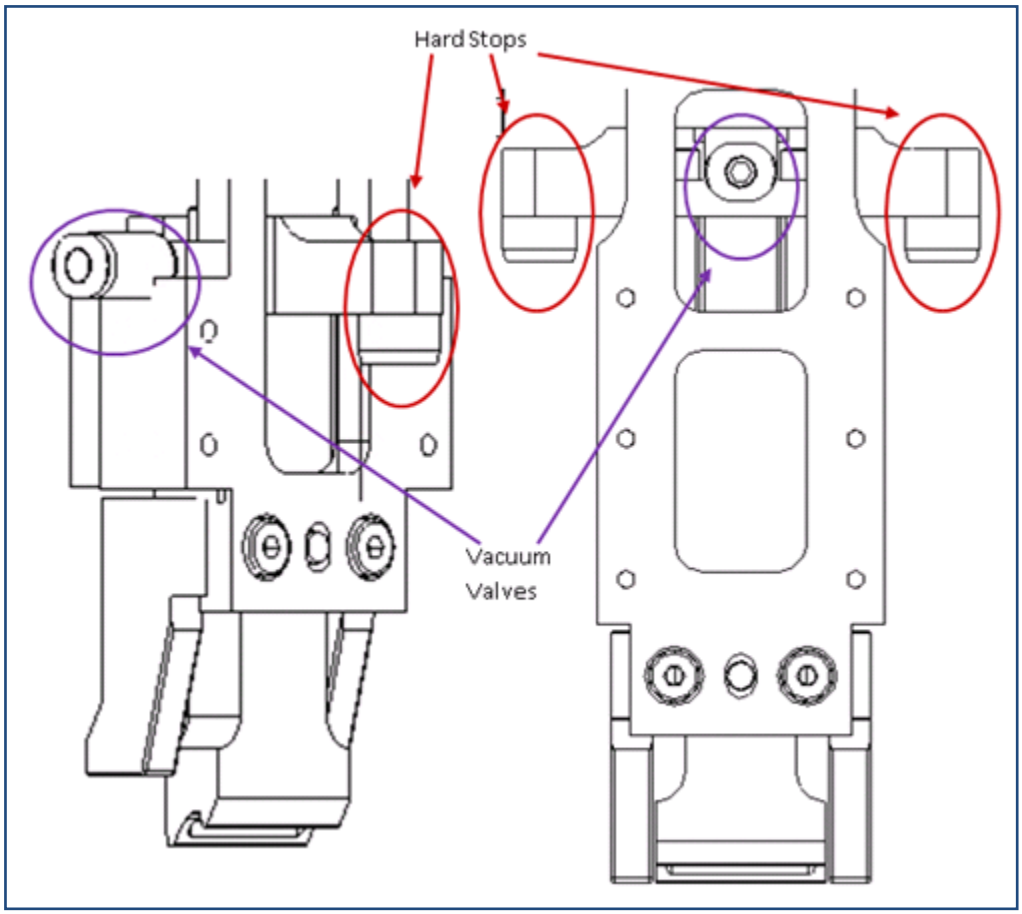

a) Original Vacuum Head Cap **b) Redesigned Vacuum Head Cap**

In order to allow for this modification, the hard stops had to be moved upward and in this assembly. A design was formulated, which allowed for the hard stops to be mounted on a front plate. This new hard stop design can be seen below:

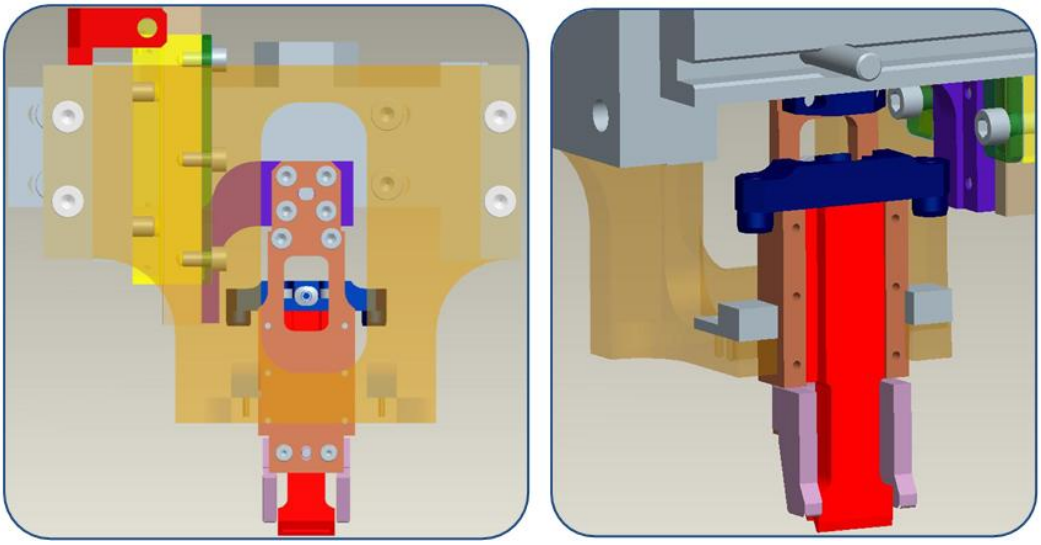

Initial Weldment redesign (front and isometric views)

There are tradeoffs whenever a design is altered. An initial analysis shows that while the changes will greatly reduce the chance of binding, several other properties are affected as well. The effective mass of the system increases 7.7% (6.832 kg to 7.355kg) while the effective stiffness decreases 9.2% (18.7 MN/m to 17 MN/m). The cam-closure dynamic forces are affected by the alterations as well. The maximum force increases 1.2% and the minimum force decreases 1.9%. A pro of this design was that the impact would be moved from the rail to the station itself, eliminating future damage to this precision rail and making it easier to adjust the mechanism upon final assembly.

After a design review and discussions with our sponsor, there were concerns expressed that the front-plate attachment for the hard stop anvils could be problematic since it restricted the visibility of the vacuum head. To address this concern, we decided to redesign the mounting weldment so that the hard stop anvil rested on the weldment directly.

8.3 Appendix E – Digital Media

A complete CAD assembly, detailed CAD models, and part drawings are provided separately on the accompanying CD.